TAMPERE UNIVERSITY OF TECHNOLOGY

Jari Nikkinen

ADVANCED PULSED AND LONG-WAVELENGTH SEMICONDUCTOR LASERS BASED ON QUANTUM-DOT AND ANTIMONIDE MATERIALS

MASTER OF SCIENCE THESIS

Examiner: Professor Oleg Okhotnikov
The subject was approved by
the department council on
April 20th, 2011

TIIVISTELMÄ

TAMPEREEN TEKNILLINEN YLIOPISTO
Teknis-luonnontieteellinen koulutusohjelma
JARI NIKKINEN: Advanced pulsed and long-wavelength semiconductor lasers based on quantum-dot and antimonide materials
Diplomityö, 41 sivua, 2 liitesivua
Marraskuu 2014
Pääaine: Teknillinen fysiikka
Tarkastajat: Professori Oleg Okhotnikov
Avainsanat: puolijohde kiekko laser, muotilukittu reunasta emittoiva laser diodi, kvanttikaivo, kvanttipiste, galliumantimoni, galliumarsenidi

Tämän työn tarkoituksena on tutkia puolijohdekiekkolaseria joka emittoi valoa 2.5 μm aallonpituudella ensimmäistä kertaa [28; 26]. Vaikka laser diodeja on jo raportoitu vastaavalla aallonpituudella, on työn motivaationa tuoda myös kiekkolaserin emissio aallonpituus tälle alueelle. Puolijohdekiekkolaserin etuna verrattuna laser diodeihin on niiden ylivoimainen optisen säteen laatu ja tehoskaalattavuus. Lisäksi sillä on paremmat käytännön ominaisuudet aallonpituuden säädettävyyteen. Nämä ominaisuudet ovat iso etu monissa sovelluksissa kuten kemiallisissa antureissa, biolääketieteessä, termisessä kuvantamisessa ja spektroskopiassa.

Työssä tutkittiin myös muotolukittuja reunasta emittoivia 1.2 μm ja 1.3 μm kvanttipistelaserdiodeja. Näiden tutkimisen tarkoituksena oli käyttää niitä pulssin lähteenä vismuttikuituvahvistimille, jotka perustuvat verrattain uuden tyyppisiin aktiivisiin kuituihin. Motivaationa tälle työlle oli löytää kompakti ratkaisu laserista, jossa lyhyiden pulssien ja nopea toistotaajuuden omaavaa valoa voisi vahvistaa säilyttäen hyvän säteen laadun.

Tämän työn tutkimukset toteutettiin empiirisesti eli kokeellisesti. Ensimmäisenä puolijohdekiekkolaseri prosessoitiin. Seuraavaksi suunniteltiin koejärjestelyt ja lasereiden optiset ominaisuudet mitattiin erinäisillä instrumenteilla.

Ensimmäistä kertaa maailmassa, tässä työssä saatiin demonstroitua optisesti pumpattu puolijohdekiekkolaseri joka toimii 2.5 μm aallonpituudella. Laserin maksimitehoksi saavutettiin 600 mW jatkuvatoimisena. Aallonpituuden säädettävyydeksi saavutettiin jopa 130 nm maksimi tehon ollessa 310 mW.

Johtopäätöksenä tuloksista voidaan sanoa, että suuritehoisten kiekkolasereiden tekniikka voidaan vielä pidemmällekin kuin 2.5 μm käyttämällä (AlGaIn)(AsSb) yhdistepuolijohteita. Lisäksi nämä materiaalit mahdollistivat leveäkaistaisen pienihäviöisen puolijohdepeilin valmistamisen , mikä on tavoiteltua aallonpituussäädettäville lasereille. Muotolukitut reunasta emittoivat kvanttipistelaserit saatiin tässä työssä karakter-

isoitua tarkoin vismuttikuidun tarpeisiin. Parhaillaan 1.2 μm laser diodi tuotti 71 mW tehoa, 5.56 ps pulsseilla ja 30.45 GHz toistotaajuudella. Vastaavasti 1.3 μm laser diodille saatiin tuloksiksi 20.4 mW, 8.3 ps ja 10.2 GHz. Molempien lasereiden tapauksessa nämä tulokset saatiin lasereiden toimiessa perustilalla. Johtopäätöksenä voidaan näiden lasereiden sanoa sopivan hyvin pulssilähteiksi vismuttivahvistimille. Vaikka pulssilaserit toimivatkin erinomaisesti, havaitsimme että vismuttivahvistimet vaatisivat vielä paljon kehittämistä tulevaisuudessa.

ABSTRACT

TAMPERE UNIVERSITY OF TECHNOLOGY
Master's Degree Programme
JARI NIKKINEN: Advanced pulsed and long-wavelength semiconductor lasers based on quantum-dot and antimonide materials
Master of Science Thesis, 41 pages, 2 Appendix pages
November 2014
Major: Advanced Engineering Physics
Examiner: Professor Oleg Okhotnikov
Keywords: semiconductor disk laser, mode-locked edge-emitting laser diode, quantum well, quantum dot, galliumantimonide, galliumarsenide

In this thesis mid-infrared optically-pumped semiconductor disk laser (OP-SDL) emitting at 2.5 μm is developed for the very first time. Although laser diodes at this wavelength have already been reported, the motivation of this experiment is to extend the first SDL to this region. The advantage of SDLs over laser diodes is their superior beam quality with high powers, and practical potential for wavelength tuning. These properties are a great asset in many applications such as chemical sensing, biomedicine, thermal imaging and spectroscopy.

Mode-locked quantum dot edge-emitting lasers emitting at 1.2 μm and 1.3 μm are also investigated in this thesis. The purpose of these experiments is to use them as master oscillator for bismuth doped fiber amplifiers, operating at 1.2–1.3 μm. The motivation of these experiments was to build a compact system to achieve amplified short pulses with good beam quality.

Studies in this thesis were carried out experimentally. First, the SDL chip was processed and build into a laser. Then the laser output properties were measured with various instruments.

For the first time, a GaSb-based OP-SDL operating at 2.5 μm spectral range has been demonstrated. The laser operated in continuous wave as well as tunable laser. With an intra-cavity diamond heat spreader used for thermal management, 600 mW of continuous wave output power has been achieved with good beam quality. Tunable operation with 130 nm tuning range and output power up to 310 mW has been obtained, limited by the free spectral range and loss induced by the etalon.

As a conclusion, the obtained results show that the advantages of high-power disk laser technology can be extended to 2.5 μm and beyond utilizing (AlGaIn)(AsSb) semiconductor compounds. This material system was found to provide both wide band low loss mirrors and wide gain desired for tunable lasers. These characteristics allow high power and high brightness to be achieved.

The mode-locked edge-emitting quantum-dot lasers operating at 1.2 μm and 1.3 μm spectral range have been characterized in detail. For the 1.2 μm laser diode, the optimum performance resulted in 71 mW of average output power with 5.56 ps pulse width and 30.45 GHz repetition rate. Respectively, the 1.3 μm laser diode reached 20.4 mW of output power and 8.3 ps pulse width at 10.2 GHz pulse repetition rate. For both laser diodes stable mode-locking was found to originate from ground state lasing. As a conclusion, it is shown that mode-locked edge-emitting lasers can be used as a compact ultra fast seed signal source for Bi-fiber amplifiers. Although the seed lasers themselves operated as planned, it was concluded that the Bi-amplifiers would still need further development.

PREFACE

This work has been carried out at the Optoelectronics Research Centre (ORC) of Tampere University of Technology.

First of all, I want to thank Professor Markus Pessa for giving me the opportunity to work here in the superior scientific environment.

I want show my deepest gratitude to the examiner of this thesis, Professor Oleg Okhotnikov. Without his expertise and guidance, this work would not have been possible.

I want to thank all my colleagues at the ORC, especially M.Sc. Jussi Rautiainen and M.Sc. Esa Saarinen deserves the greatest recognition of all. Thank you for your first hand guidance throughout my work at the ORC. A great acknowledgment belongs to the crystal growers Ph.D. Soile Suomalainen, M.Sc. Jonna Paajaste and Riku Koskinen for fabricating the semiconductor structure of the disk laser used in this work.

Big recognition for providing me edge-emitting lasers goes for M.Sc. Daniil Nikitichev and Division of Electronic Engineering and Physics at the University of Dundee.

Big thanks belong to Ph.D. Antti Härkönen, who has helped me enormously in many ways. I want to thank Antti Rantamki for valuable discussions and for the help they have given me on the technical issues. Thanks for Juho Kerttula, Regina Gumenyuk, Alexander Chamorovskiy and all the people at the Ultrafast and intense optics group.

Finally, I would like to thank my family for the love and support they have given throughout my studies.

Tampere, November 19th, 2014

Jari Nikkinen

CONTENTS

1. Introduction 1
2. General features of semiconductor lasers 3
2.1 Semiconductors as active material 3
2.2 Pumping schemes 4
2.3 Waveguide and resonator optics 5
2.3.1 Ray, wave, free-space and resonator optics 5
2.3.2 Free-space propagation 7
2.3.3 Free-space resonators 9
2.3.4 Distributed Bragg reflector 9
2.3.5 Fabry–Pérot interferometer 10
3. Optically pumped semiconductor disk lasers based on quantum-wells . . . 11
3.1 Structure of the gain mirror 11
3.2 Thermal management and processing 12
3.3 Gallium antimonite based semiconductor materials 13
3.4 Properties of optically-pumped semiconductor disk lasers 14
3.4.1 Beam quality 14
3.4.2 Power scaling 14
4. Edge-emitting semiconductor lasers 16
4.1 Structure of edge-emitting diode lasers 16
5. Research methods 19
5.1 Power measurements 19
5.2 Wavelength measurements 20
5.3 Beam characterization 20
5.4 Pulse duration measurements using autocorrelation 21
6. Experiments and results 22
6.1 Experiments of 2.5 μm semiconductor disk laser 22
6.2 Results of 2.5 μm semiconductor disk laser 24
6.2.1 Power scaling and beam quality 24
6.2.2 Tuning results 26
6.3 Experiments of mode-locked edge-emitting laser 27
6.4 Results of mode-locked edge-emitting laser 28
6.5 Experiments with Bi-amplifier results 35
6.6 Results of Bi-fiber amplifier 36
7. Conclusions and future work 40

A. Appendix 47

ABBREVIATIONS AND SYMBOLS

Abbreviations

$ABCD$-matrix	A matrix describing optical element, ray-transfer matrix
AC	Autocorrelation
Al	Aluminum
AR	Anti-reflective
As	Arsenide
Bi	Bismuth
CCD	Charge-coupled device
DBR	Distributed Bragg Reflector
Ga	Gallium
HR	High reflective
In	Indium
LPE	Liquid-phase epitaxy
MBE	Molecular-beam epitaxy
MIR	Mid-infrared
MOCVD	metal-organic chemical vapor deposition
MOPA	master oscillator power amplifier
NA	Numerical aperture
OC	Output coupler
OPL	Optical length
OP-SDL	Optically-pumped Semiconductor disk laser
PGS	Periodic gain structure
PID	A proportional-integral-derivative (controller)
QD	Quantum dot
QW	Quantum well
RoC	Radius of curvature
RPG	Resonant periodic gain
Sb	Antimony
SDL	Semiconductor disk laser
SiO_2	Silicon dioxide
SPCVD	surface-plasma chemical vapor deposition
TiO_2	Titanium dioxide
VPE	Vapor-phase epitaxy

Symbols, Greek alphabet

λ	Wavelength
ω	Frequency
k	Wave vector
ϕ	Phase of a wave
Ψ	Wave package
θ_i	Angle
E_g	Energy gap between valence and conduction bands
E_n	Quantized energies, where $n = 1, 2, 3, \ldots$
$\hbar$	Planck constant over 2π
d	Thickness
r_i	Radial displacement or radius
M_i	Ray-transfer matrix
M^2	Beam quality factor
q	Gaussian beam q-parameter
R	Wave front radius of the beam
w	Width parameter
I	Intensity
P	Optical power
$STAB$	Stability value for optical cavity
N	Number of layer pairs
$\Delta\nu_{\mathrm{FSR}}$	Free spectral range in frequency domain
$\Delta\lambda_{\mathrm{FSR}}$	Free spectral range in wavelength domain
c	speed of light
L	Optical length
P_{SHG}	Optical power of second harmonic generation

1. INTRODUCTION

Since the invention of the first laser and a long history of laser research, lasers have become an important part of our everyday life in modern societies. The vast array of different types of lasers covers many kind of applications from industrial, medical and military needs to consumer electronics.

Different laser types are typically first categorized by their active material into solid-state, semiconductor, gas, liquid etc. lasers. Secondly, lasers can be categorized by their design, such as disk lasers or edge-emitting lasers. Thirdly, they can be categorized by their output properties into pulsed, continuous wave or tunable lasers. In this thesis 2.5 μm semiconductors are used as active material. More precisely, in this thesis gallium antimonides (GaAs) are used for 2.5 μm wavelength and quantum dots for 1.2-1.3 μm pulsed lasers due to their suitable properties.

For optoelectronic devices operating in the mid-infrared spectral range, the nearly lattice-matched III-V semiconductor material system (AlGaIn)(AsSb) establishes a firm platform. Lattice-matched or strain-compensated structures employing InGaAsSb as the quantum wells and AlGaAsSb for barrier and spacer layers grown on GaSb substrates are demonstrated to be the best choice for long-wavelength semiconductor lasers and photodetectors. Their applications include chemical sensing, biomedicine and thermal imaging [28; 26].

Optically-pumped semiconductor disk laser (OP-SDL) is a concept where the surface of the thin semiconductor disk is realized perpendicularly to the emission direction and pumping is implemented optically. The primary advantage of such laser compared with in-plane diode lasers is an improved mode control, which enables high output power with diffraction-limited beam quality [28; 26]. The GaSb system is particularly suitable for lasers with vertical-cavity configuration since this material system enables for lattice matched distributed Bragg reflectors (DBRs) comprised of layers with a high refractive-index contrast. Such DBRs have an exceptionally broad stop-band and require a relatively small number of layer pairs to achieve high reflectance. The broad stop-band makes GaSb-based vertical-cavity lasers highly promising for spectroscopic application requiring a wide tuning range.

Quantum dots are a concept where dots of lower band gap semiconductor material

are embedded into higher band gap material. In such a system electron-hole pairs are confined into these dots in 3-dimension so that the density of states becomes discrete lines, and the dots behave like energy levels of a single atom. Furthermore, the variation of the dots broadens the overall gain spectrum. This is extremely important aspect for mode locking where wide gain spectrum is needed. Broad gain spectrum is an asset also for wavelength tuning. Last, but not least, wavelength shift due to temperature in quantum dots is small compared to other semiconductors, which makes it a good choice for applications where wavelength stability is needed.

When it comes to pulsed lasers there are several ways to achieve short optical pulses. Mode-locking is the technique for generating ultra-short optical pulses. Mode-locking can be attained either by active or passive means. Active techniques use an external modulator, whereas in passive techniques the pulse regime is initiated through the action of a saturable absorber placed in the laser cavity. Passive schemes usually lead to more compact systems and shorter pulses.

The purpose of this thesis is to investigate for the very first time [28; 26] a galliumantimonide based semiconductor disk laser emitting at 2.5 μm. The investigation of the SDL includes power scaling, beam quality and wavelength tuning. Furthermore, mode-locked quantum dot edge-emitting lasers emitting at 1.2 μm and 1.3 μm are investigated as master oscillator for bismuth doped fiber amplifiers. The approach in this thesis is very experimental including processing of lasers, setup designing and building, and characterization of the laser output properties.

2. GENERAL FEATURES OF SEMICONDUCTOR LASERS

A laser can be considered to consist of three elements: an active material as gain, a pumping scheme, and an optical feedback system as in an amplifier or a resonator as in laser oscillator [40; 41]. In this chapter these features are described in a level that is common to the lasers studied in this thesis.

2.1 Semiconductors as active material

Semiconductors are materials where the energy levels take the form of groups of closely spaced levels that form bands. These bands are called valence band and conduction band separated by an energy gap E_g. In the absence of thermal excitations, these are either completely occupied by electrons or completely empty. Fundamental optoelectronic properties are mainly understood from two processes between these bands. First, absorption of a photon can create an electron-hole pair, and second, the recombination of an electron and hole can result in the emission of a photon. [36]

Semiconductors can be further divided into direct and indirect band gap materials. In the direct band gap material momentum of electrons is not changed during recombination and is thus efficient light emitters. Further assuming that in equilibrium electrons and photons are in the lowest energy levels, recombination of electron-hole pairs then takes place from lowest energy in conduction band to highest energy in valence band. As a result, the emission photon energy matches closely to the band gap energy. [36; 18]. In this thesis, direct gap semiconductors, ternary InGaAs and quaternary AlGaAsSb/GaInAsSb alloys are considered. Such alloy have also advantage that band gap can be varied by varying the material composition within certain limits.

By means of epitaxial growth methods, such as molecular-beam epitaxy (MBE), liquid-phase epitaxy (LPE), vapor-phase epitaxy (VPE), metal-organic chemical vapor deposition (MOCVD), it is possible to grow very thin layers of semiconductors. If very thin layer of low band gap material is placed between two higher band gap

barriers the energy-momentum relation for a bulk semiconductor material no longer applies. "Thin" in this case means that the layer thickness is smaller than, the de Broglie wavelength of electrons [36]. In such case the electrons and holes can be considered to be in a potential well or a quantum well (QW). For a particle in a 1D infinite potential well, it is known that the quantized energies for the particle become

$$E_n = \frac{\hbar^2 \pi^2 n^2}{2md} \tag{2.1}$$

where $\hbar$, is the Planck constant over 2π, $n = 1, 2, 3, \ldots$ is the quantum number, m is the particle mass and d is the thickness of the well. [36; 41]

In real life with semiconductors infinite potential wells cannot be achieved. However, the photon emission is most probable from the lowest energy levels for which the equation (2.1) is a very good approximation. Moreover, the particle mass has to be treated as an effective mass of electrons and holes in conduction and valence bands respectively, and thus their energies must be treated separately. The overall emission energy is then the sum of band gap, valence band and conduction band energies. It is also now seen that the wavelength of such material structure can be tailored readily by changing the band gap and layer thickness of the quantum well layer.

Other advanced semiconductor structures are quantum wires, where potential barriers are valid in 2 dimension, and quantum dots (QD), where potential barriers forms a box in all 3 directions. The more dimensions there is involved the more conduction and bands split into overlapping sub-bands, and in QDs the electrons are already so narrowly confined that the allowed energy levels become discrete. Because of such atom-like discrete energy levels QDs are sometimes referred to as artificial atoms. [36]. In principle, QDs produces a very narrow bandwidth but in practice manufacturing of QDs forms large variety of dot sizes resulting in a strong Gaussian broadening of the active material. Thus, QDs provide a wide gain bandwidth which is desirable for tunable and pulsed lasers. [34]

2.2 Pumping schemes

Both electrical and optical pumping is used in semiconductor lasers. Optical pumping is simply achieved by the use of external light with photon energies larger than the energy gap of the semiconductor material. [29]. Pump photons are then absorbed resulting in the generation of electron-hole pairs, and steady-state popula-

tion inversion. [36]. In the electrical pumping, on the other hand, electrons and holes are injected directly into a p-n junction with a forward bias. Electrons and holes are then radiatively recombined in the active area between the p- and n-doped semiconductors.

One important advantage of optical pumping is that by proper gain design the pump can be absorbed only by certain pump absorbing layers placed close to the quantum wells or quantum dots. This provides efficient and more importantly, uniform pumping in a well confined area. In addition to cavity design and thin gain region, this enables ultra-high beam quality lasers once there is no objects in the cavity causing aberrations. On the down side, optical pumping requires external pump optics and a pump laser which makes overall systems more complex compared to electrically pumped lasers. [27]

In contrast, the advantage of electrical pumping is higher efficiency and the compactness of the laser. Furthermore, it allows direct modulation of pump current. Down side of the electrical pumping lies in power limitation typically to hundreds of milliwatts in a single transversal mode operation. Or otherwise, poor beam quality with higher powers. [29]

2.3 Waveguide and resonator optics

For the laser action to occur, one needs to build up a feedback system which returns some portion of the light to the active material. In this chapter few important rules to build up a feedback system or a resonator are presented.

2.3.1 Ray, wave, free-space and resonator optics

Matrix formalism is a powerful way for ray tracing. Any ray propagating along the optical z-axis can be characterized by two parameters: radial displacement r_i from the z-axis and its angular displacement θ_i. Within the paraxial-ray approximation angular displacements are assumed to be small so that we can approximate angles as $\theta_i \approx dr_i/dz_i = r_i'$. In doing so, we may now write a matrix equation

$$\begin{pmatrix} r_2 \\ r_2' \end{pmatrix} = \begin{bmatrix} A & B \\ C & D \end{bmatrix} \begin{pmatrix} r_1 \\ r_1' \end{pmatrix}, \tag{2.2}$$

for arbitrary optical system shown in figure 2.1. The $ABCD$ matrix is also known as ray-transfer matrix. [41; 36]

Matrices for several types of common optical elements, defined in this way, are

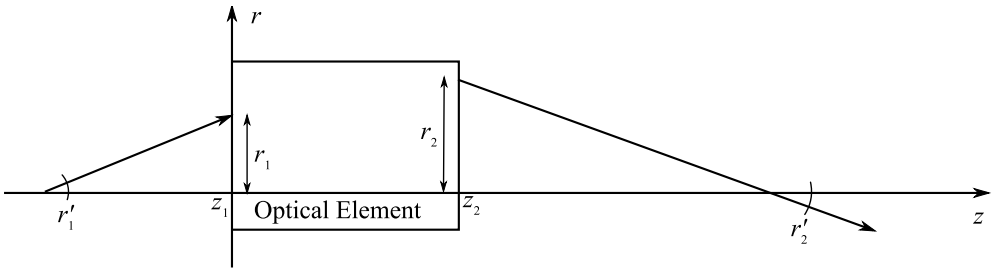

Figure 2.1: Ray parameters in an arbitrary optical element. [41]

proved in several optics books [41; 36]. For optical system consisting of several elements, one can readily write equation for whole system by simply multiplying equation (2.2) step by step with $ABCD$-matrices of individual elements from the left to right, and thus after m elements

$$\begin{pmatrix} r_m \\ r'_m \end{pmatrix} = M_m M_{m-1} \dots M_2 M_1 \begin{pmatrix} r_0 \\ r'_0 \end{pmatrix}. \tag{2.3}$$

Moreover, another useful result is that for most optical elements the determinant of the $ABCD$-matrix is $\det(M) = 1$, which allows us to write

$$AB - CD = 1. \tag{2.4}$$

If a system consists of elements obeying this law, then the determinant of the whole system matrix is a multiplication of determinants of each matrix, and thus, the system obeys the same law. [40]

Where ray optics describes propagation direction of the light within an optical system, wave optics describes field distribution of the light. For simplicity it is convenient to consider uniformly polarized monochromatic plane waves within paraxial approximation of the form

$$E(x, y, z, t) = u(x, y, z) \exp(-jkz) \exp(j\omega t), \tag{2.5}$$

where u is slowly varying amplitude. If such wave is now considered in an optical system described by the $ABCD$-matrix, then the amplitude equation in the plane (x, y, z) is obtained using Fresnel–Kirchhoff integral

$$\begin{aligned} u(x, y, z) = \ & \tfrac{j}{B\lambda} \int\int u(x_1, y_1, z_1) \\ & \exp\left\{-jk\left[\frac{Ar_1^2 + Dr^2 - 2x_1 x - 2y_1 y}{2B}\right]\right\} \mathrm{d}x_1 \mathrm{d}y_1, \end{aligned} \tag{2.6}$$

where $r^2 = x^2 + y^2$. [40]

One of the most important field distributions in laser optics is Gaussian beam having the form

$$u(x, y, z) \propto \exp\left(-jk\frac{x^2 + y^2}{2q}\right), \tag{2.7}$$

where q-parameter is called the complex beam parameter of the Gaussian beam. Substituting this into equation (2.6) and calculating the integral results as

$$u(x, y, z) = \frac{1}{A + (B/q1)} \exp\left(-jk\frac{x^2 + y^2}{2q}\right), \tag{2.8}$$

where q is related to the initial q_1 by the law

$$q = \frac{Aq_1 + B}{Cq_1 + D}. \tag{2.9}$$

The valuable meaning for q-parameter comes then from further properties of Gaussian beams. It can be shown that for Gaussian beams the q-parameter can be divided into real and imaginary parts so that

$$\frac{1}{q} = \frac{1}{R} - j\frac{\lambda}{\pi w^2}, \tag{2.10}$$

where R is the wave front radius of the beam and $2w$ is the diameter of the beam. More precisely the diameter, is the width of the amplitude field where amplitude is $1/e$ of the maximum, and since intensity $I \propto u^2$ it is the $1/e^2$-width of the intensity. [40]

2.3.2 Free-space propagation

Let us next consider some basic properties of Gaussian beams. From previous section it is easy to obtain simple equations for spot radius and wave front radius

$$w^2 = w_0^2\left[1 + \left(\frac{z}{z_R}\right)^2\right] \tag{2.11}$$

$$R(z) = z\left[1 + \left(\frac{z_R}{z}\right)^2\right], \tag{2.12}$$

where $z_R = \pi w_0^2/\lambda$ is the Rayleigh range which defines the distance in which the waist has increased by the factor of $\sqrt{2}$. From equation (2.11) it is now easy to

define a beam divergence angle due to diffraction

$$\theta_d = \frac{\lambda}{\pi w_0}. \tag{2.13}$$

Thus far only Gaussian beam has been considered. However, in real life ideal Gaussian beams are difficult to achieve. Most laser beams contain higher order spatial modes which increase the divergence and thus one may define a M^2-factor to describe the quality of the laser beam. M^2 is defined [41] by the diffraction angle

$$\theta_d = M^2 \frac{\lambda}{\pi w_0}. \tag{2.14}$$

By this definition the equation (2.11) results in equation

$$w^2(z) = w_0^2 + M^4 \left(\frac{\lambda^2}{\pi^2 w^2} \right) (z - z_0)^2, \tag{2.15}$$

where z_0 is position of the beam waist radius w_0. [41]. A plot of this function is shown in figure 2.2.

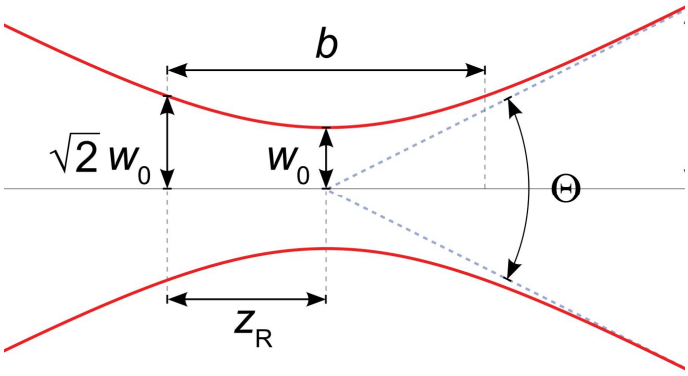

Figure 2.2: Beam waist of a Gaussian beam with M^2=1

One could say that beam quality factor M^2 measures diffraction of higher order beams. More precisely beam waist is magnified by M, the beam depth of focus is magnified by M^2, and the angular divergence is magnified by the factor M. [36]. For the lowest order Gaussian beams $M^2 = 1$ and above 1 for higher orders. Moreover, the beam with $M^2 = 1$ has the smallest diffraction angle and is thus called as diffraction limited beam. [41]

2.3.3 Free-space resonators

$ABCD$-matrices can be used to describe beam propagation in a resonator as well. For resonators roundtrip matrix is built in similar way from individual elements to form whole a system, back and forth. In order to build up a stable resonator one needs to require that the q-parameter after each round must be the same as initially, i.e. $q = q_1$. This allows q to be determined from equation (2.9). Then, requiring that the q-parameter must be complex leads to a solution

$$(D - A)^2 + 4BC < 0. \tag{2.16}$$

Further simplification can be obtained by using equation (2.4) yielding

$$-1 < \frac{D + A}{2} < 1, \tag{2.17}$$

which is well known stability law for general a resonator.

The stability law gives only the limits in which the resonator is stable. To evaluate the stability one has to derive more advanced equations. In this thesis cavity is designed with Winlase professional program which defines stability as

$$\mathrm{STAB} = 1 - \left(\frac{A + D}{2}\right)^2. \tag{2.18}$$

In this definition stability holds values from 0 to 1, 0 being unstable and 1 being perfect stability.

2.3.4 Distributed Bragg reflector

A distributed Bragg reflector (DBR) is a mirror structure which consists of an alternating sequence of layers of two different refractive indices, with optical thickness of each layer corresponding to one-quarter of the wavelength for which the mirror is designed. For a given wavelength λ_0 and even number of layer pairs, a quarter-wave mirror is the structure which gives the highest reflectivity achievable. The reflectivity of such a mirror made of materials with refractive indices n_1 and n_2 is given by equation

$$R = \left[\frac{\frac{n_0}{n_s} - \left(\frac{n_1}{n_2}\right)^{2N}}{\frac{n_0}{n_s} + \left(\frac{n_1}{n_2}\right)^{2N}}\right]^2 \tag{2.19}$$

where N is the number of layer pairs. From this equation it is immediately seen that high index contrast yields in high reflectivity. Secondly, with higher index contrast the reflection bandwidth is also wider, which often makes large index contrast a desirable feature. [45]

The reason for this behavior arises from a few fundamental laws. First of all, each interface between the two layers induces a Fresnel reflection. In addition the optical path length between reflections from subsequent interfaces is half the wavelength and the reflection coefficients for the interfaces have alternating signs. This results a constructive interference yielding a strong reflection. [45; 29]

2.3.5 Fabry–Pérot interferometer

Fabry–Pérot interferometer is an important concept in lasers. In principle, it consists of two plane, parallel, highly reflecting surfaces separated by a distance. In such a cavity, forward and backward reflected light forms a standing wave. [13]. Consequently only resonant frequencies are fully transmitted, and other frequencies are reflected. The separation of two adjacent frequencies can be written as

$$\Delta\nu_{\mathrm{FSR}} = \frac{c}{2L}, \tag{2.20}$$

and in similar way in relation to wavelength this equation can be written as

$$\Delta\lambda_{\mathrm{FSR}} = \frac{\lambda^2}{2L}, \tag{2.21}$$

where c is the speed of light and $L = nd$ is the optical length of the Fabry–Pérot interferometer. [13]. These equations are known as free spectral range (FSR).

Significance of the Fabry–Pérot interferometer arises in various cases in lasers. First of all, all expect ring cavity lasers, forms itself a Fabry–Pérot cavity. Secondly, lasers such as disk lasers typically consist of gain disk with parallel surfaces thus comprising a Fabry–Pérot sub-cavity within the laser cavity. Moreover, one can place a Fabry–Pérot etalon into the cavity, case which is discussed in more detail in chapter 6.2.2.

3. OPTICALLY PUMPED SEMICONDUCTOR DISK LASERS BASED ON QUANTUM-WELLS

An optically-pumped semiconductor disk laser (OP-SDL) is a laser concept where laser amplification is created perpendicular to the semiconductor wafer surface and pumping is realized optically. In this chapter, an overview of the SDL used in this thesis is described.

3.1 Structure of the gain mirror

The gain mirror of a semiconductor disk laser consists of a gain section and a highly reflective mirror, integrated together. In addition it may include partially reflective top mirror or even anti-reflection coating. In this thesis, the gain mirror consists only of a gain and a mirror.

The gain mirror reflector is usually a DBR described in chapter 2.3.4 and is fabricated of lattice matched semiconductor layers. To prevent absorption losses such mirrors are fabricated of high band-gap semiconductors. Amount of DBR layer pairs of the mirrors depends on the refractive index difference of the suitable materials and thus can vary from few tens to several tens of layer pairs. As an example, GaSb/AlAsSb pairs have refractive indexes of 3.875 and 3.158 respectively. For such layers grown on GaSb substrate, one can calculate from equation 2.19 that with 21 layer pairs alone reflectivity of 99.9 % can be achieved. Here the mirror is assumed to be on the interface with semiconductor substrate having $n_0 = 3.158$. Moreover, depending on refractive index of following gain section layers the DBR might require an extra quarter-wave thick layer in order to obtain highest reflectivity, as is the case in this thesis.

In OP-SDLs quantum wells, that provide gain to the optical wave, are formed by thin semiconductor layer between two higher band gap semiconductor barriers. The pump photons are absorbed in barrier layers creating excited carriers i.e. electron-hole pairs. These carriers then diffuse to the smaller band gap quantum well and then recombination in a quantum well supports laser action. One advantage of such system is that it allows independent optimization of pump absorption and

gain. Moreover, semiconductor-air interface and bottom DBR forms a Fabry–Pérot micro-cavity which can support a standing wave in the gain section. To obtain efficient gain, quantum wells can be placed into the anti-nodes of the standing wave, as can be seen in figure 3.1. Such arrangement is referred to as resonant periodic gain (RPG) [27] or simply periodic gain structure (PGS) [5]. [27]

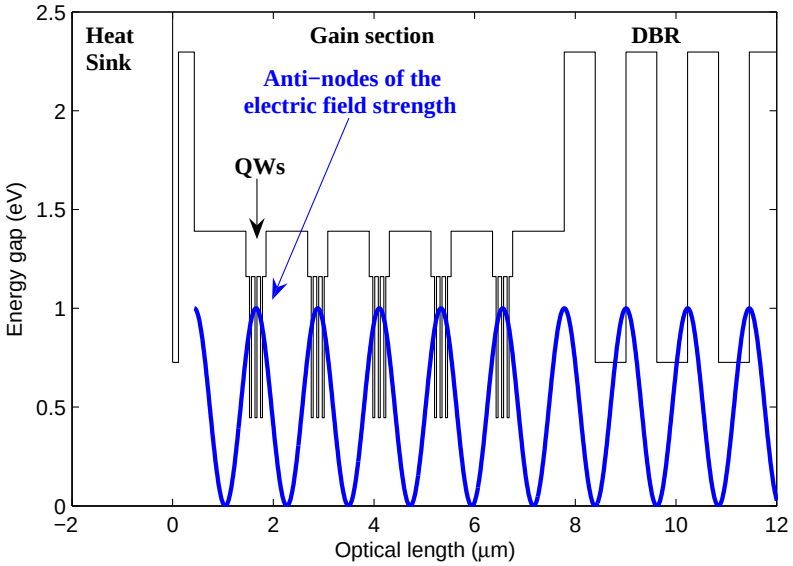

Figure 3.1: Energy gap diagram of the gain mirror used in this work

In addition to quantum well structures SDLs typically have a high bandgap window layer on the top of the structure to prevent carrier diffusion to the top surface. Carrier diffusion away from the quantum wells could result in increased nonradiative recombinations and thus reduced gain. [27].

3.2 Thermal management and processing

Thermal effects are often the reasons for power limitation and overall device performance of SDLs, and thus proper thermal management is crucial [19]. For managing with excessive heating of the gain medium, there are two main approaches to counteract this problem. The other is so called ”flip-chip” approach and the other is intracavity heat spreader approach. The choice of approach leads to two distinct ways of processing. In this thesis the latter is used for its simplicity.

In the intra-cavity heat spreader approach a transparent thermally conductive crystal is bonded directly onto the surface of the gain chip. This method has the advantage that the cooling is obtained very close to the active layers without thermal resistance of the substrate and DBR. [19]. However, once heat spreader is placed

into the cavity it sets conditions for the optical quality. It has to be transparent, non-absorbing, often non-birefringent and good surface-grade together with high thermal conductivity. One such material that obeys all these conditions along with superior thermal conductivity is diamond. However, diamonds are rather expensive which makes large scale manufacturing expensive.

The processing steps of intra-cavity heat spreader approach are rather simple which goes in general terms as follows. After growth, the wafer is cleaved into square pieces of few millimeters in size. Then cleaned diamond and gain chip are capillary bonded together with water. Capillary bonding ensures that the surfaces are pulled tightly together by Van der Waals force, providing efficient contact for heat transfer from the gain chip to the diamond. This is the utmost important step in the process and it requires surfaces to be clean, ultra-smooth and flat [6]. Such unity of gain chip and diamond is further mounted to a copper heat sink which also protects the stack. Moreover, to ensure good heat dissipation to copper block, thin and soft indium foil is used between copper-diamond and copper-gain chip interfaces.

The flip-chip process on the other hand is more complex, and goes roughly as follows. First, the epitaxial growth is realized in opposite order: gain section first, DBR second, from which the name flip-chip. In this process the chips are then soldered from DBR side to a heat sink using metal solder. The substrate on the top of the stack is then removed by an etching process. The overall process is, however, far more complicated than that, and due to the side effects that may occur from soldering and etching this approach is not recognized in this thesis. In comparison to intracavity diamond approach, the heat is transferred through a thick DBR section which causes thermal resistance and is usually a bit less efficient than diamond approach.

3.3 Gallium antimonite based semiconductor materials

It has been already shown with diode lasers that GaInSb and GaInAsSb quantum wells enable 1.9–3.3 μm emission wavelengths [24]. There are numerous applications that can benefit from this wavelength range. First of all there are several particularly important gases exhibiting specific absorption lines at wavelengths between 2.0 μm and 3.0 μm. This makes mid-infrared (MIR) lasers attractive possibility to investigate these molecular rotational-vibrational oscillations or as gas sensing applications. [9]. Secondly, combined to superior beam quality and high output powers of SDLs, this material system gives an advantage to use it in several applications, such as free-space optical communication, standoff detection, and infrared counter

measures [42]. [27]

The gallium antimonite based quaternary semiconductor $Al_xGa_{1-x}As_ySb_{1-y}$ offers two major advantages for disk lasers. First, it is ideal material for barrier, window, and absorbing layers. And secondly, large refractive index difference of $AlAs_{0.08}Sb_{0.92}$/GaSb layers provides efficient wideband distributed Bragg reflectors. These layer stacks are typically grown lattice matched to avoid high strain thick layers at MIR SDLs. [27; 44]

On the other hand, quaternary semiconductor $Ga_xIn_{1-x}As_ySb_{1-y}$ is used as active layer for two reasons. It has a direct band gap for all compositions and it is lattice matched to GaAs whenever composition satisfy the condition $y = 0.913(1-x)$. From these reasons it can also be seen that designing is more flexible with quaternary alloys than with ternary alloys. Merely by changing alloy compositions one can adjust band gap, strain, etc. individually. [39]

3.4 Properties of optically-pumped semiconductor disk lasers

In this chapter a few main properties are introduced. These properties of interest in this thesis are beam quality, power scaling and wavelength tuning.

3.4.1 Beam quality

Beam quality is very important property of OP-SDLs. Their cavity design and thin gain enables these lasers to operate with a circular beam, fundamental transverse mode TEM_{00}, and diffraction limited beams. In last decade several high-power SDLs have been demonstrated [6; 21], and even as high as 4 W diffraction limited output with $M^2 < 1.15$ [12].

Other advantage included to cavity design is the control of the cavity mode size to be matched with the pump spot size. If the pump spots size is larger than the cavity mode, then higher gain area is excited allowing higher order modes to occur. On contrary, if the pump spot is smaller, then it constrains the cavity to the fundamental mode. However, in this case outer edges of the mode are not pumped which results as a reduced power. Optimally matched spot sizes however gives higher gain stabilizing fundamental mode operation. [24]

3.4.2 Power scaling

There are two main effects that drive gain reduction at high temperature, which limits the maximum output power. First of all, the peak gain of the QWs decreases

as the temperature rises due to increased non-radiative recombination and hot carrier leakage [14]. Secondly the gain spectra tunes to longer wavelengths (red-shift) spectrally misaligning the anti-nodes of the electric field in respect to the QWs in the resonant periodic structure of the gain mirror. On the other hand, optical thickness is also increased due to increase of refractive index as a function of temperature, which slightly compensates the misalignment. However, the red shift of the gain is far more rapid than the increase of optical thickness thus eventually leading to roll over of the power. [19; 21; 33; 20; 27]

Thermal load in the SDLs is mostly induced by the quantum defect[1] and power is limited by this factor in most cases. Sometimes optical damage, thermal lens, or lateral lasing can also limit the power. The flexibility to adjust the mode size at gain, gives an opportunity to increase heat dissipation through larger mode area. The heat flow from the gain to the heat sink is essentially one-dimensional after all. However, at some point there is a limit when heat flow becomes 2-dimensional and spot size cannot be increased anymore. Furthermore, larger spot size also increases threshold pump power and thus requires higher power from the pump source. [19; 27]

Last but not least, it is good to point out that the thermal lens is not concerned in this thesis. In any case, by proper cavity alignment this minor effect can be easily minimized. Another remark is also that the wavelength of the pump source must be properly chosen in order to minimize the quantum defect. However, this might be limited by available pump sources of sufficient power and low cost.

[1] quantum defect is the energy difference of the pump and signal photons

4. EDGE-EMITTING SEMICONDUCTOR LASERS

Edge-emitting lasers are form of diode lasers where the light propagates in a direction along the wafer surface of the semiconductor chip and is reflected or coupled out at a cleaved edge of the chip [29]. In this chapter overview of the edge-emitting lasers used in this thesis are described.

4.1 Structure of edge-emitting diode lasers

It was stated in section 2.2 that radiation can be achieved from biased p-n junction. In a single p-n junction however, the active area is limited into a very narrow junction. To increase the active area in p-n junction an intrinsic semiconductor can be used between p- and n-doped layers. Such a structure is called p-i-n structure. Furthermore p-i-n structures are typically double heterostructures where p- and n-layers are made of higher band gap materials, which act as barriers and, thus the carriers are well confined in the intrinsic section. [22; 29]

Within the edge-emitting laser structure, the laser beam is guided in a waveguide structure. Typically, the wavequide is the double heterostructure, which restricts the generated carriers to a narrow region and at the same time serves as a waveguide for the optical field. This arrangement leads to a low threshold pump power and high efficiency. Depending on the waveguide properties, particularly its transverse dimensions, it is possible either to obtain an output with high beam quality but limited output power, or high output power with poorer beam quality. [22; 32]

If the active layer is made thin enough, like quantum wells quantum dot layers, this means that the vertical variation of the electron's wave function is quantized. The efficiency of a quantum well (or QD) laser is greater than that of a bulk laser because the density of states function of electrons in the quantum well (or QD) system has an abrupt edge that concentrates electrons in energy states that contribute to laser action. The problem with the simple quantum dot diode layer described above is that the thin layer is simply too small to effectively confine the light. To compensate, another 2 layers are added to form a wavequide as it is seen in figure

4.1. [22; 32]

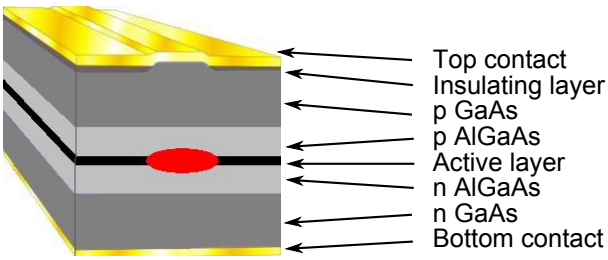

Figure 4.1: Structure of a typical edge-emitting laser diode.

A typical structure of edge-emitting laser diode described above is shown in figure 4.1. Active layer is in the middle surrounded by 2 p- and n-doped layers which form the waveguiding for the optical field. The top contact is in contact to top p-doped layer only through very narrow ridge or stripe, which injects electrons to the active area, and the laser becomes injection guided (gain guided) in horizontal direction. [22; 32]

The cavity of the edge-emitting laser diodes is formed between the end facets. Typically the Fresnel reflection from the facets is high enough for diode to start lasing. However, the light is typically coupled out from just one edge by coating the facets. Another coated with highly reflective coating, and the other with anti-reflection coating. [29]

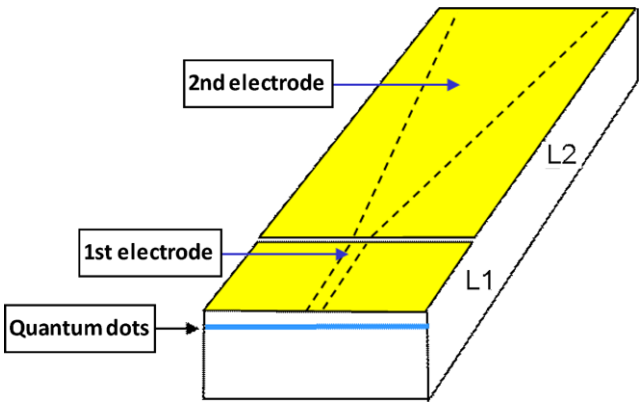

Figure 4.2: Schematic structure of advanced tapered edge-emitting laser diode. [25]

The output power of a typical laser diode is limited by their limited size of active area. To overcome this problem tapered laser diodes has been proven to be good choise. A schematic structure of a 2 section tapered laser diode is shown in figure 4.2. Tapered lasers typically consist of a straight ridge-waveguide section coupled to

a tapered section. While the straight waveguide acts as a spatial filter in the cavity, the tapered section of increasing width delivers high power. [8; 25; 2]

5. RESEARCH METHODS

In this thesis, the physical parameters, characteristics and figures of merit are the backbone to determine the quality and properties of the studied lasers. Thus the research methods concentrate on measuring the physical properties of the lasers. In this chapter basic principles of the measurement devices are described along with measurement accuracies.

5.1 Power measurements

The two most substantial parameters of lasers are output power and wavelength. For power measurements there are two practical types of power meters with individual properties; thermal sensors and photodiodes.

A thermal sensor is a good choice for most power measurements due to its rather universal specifications. It has typically wide spectral range from ultraviolet to far infrared regions, and secondly it can measure very high powers of both continuous wave as well as pulsed. The only disadvantage of such sensors is their slow response time in range of seconds, which however is not a problem measuring stable average powers of lasers.

In this thesis Ophir 3A-FS thermal sensor was used for 2.5 μm SDL's power measurements. It has suitable properties for such a laser covering spectral range from 0.19 μm to 20 μm, and power range from 30 μW to 3 W with an accuracy of ± 3 %. [23]

Photodiode based power meters on the other hand are spectrally narrower and usually limited to lower powers, but are more accurate and can be very fast. In addition to integrating sphere such power meters can accurately measure the sum of the entire ambient light incident on a small circular aperture and measure the total power in a laser beam, with best available independence of beam details such as beam shape, incident direction, and incident position. Such a sensor is therefore suitable for low power diode lasers with poor beam quality.

In this thesis Lightwave ILX OMH-6708B InGaAs integrating sphere was used for studies of ML edge-emitting lasers and Bi-doped fiber amplifiers. It has a power

range from 10 nW to 100 mW with accuracy of ±5 % and spectral range from 800 nm to 1600 nm. [3]

5.2 Wavelength measurements

The operation wavelength of a laser is as important output character as power. Optical spectrum analyzer (OSA) can be used to characterize the output spectrum of a laser. In the simplest form OSA consist of a monochromator, typically diffraction grating, slit and a photodiode which measures optical power as a function of wavelength. Due to wide range of wavelengths 3 different OSAs were used in this thesis.

In 2.5 μm continuous wave studies Yokogawa AQ6375 OSA was used with a resolution of better than 0.1 nm. Its spectral range was limited to 2.5 μm and thus another OSA was needed for tunability studies of 2.5 μm SDL. APE WaveScan has a spectral range up 2.6 μm but has lower resolution of 0.2 nm. For the edge-emitting laser and fiber amplifier studies an Ando AQ6317C OSA was used with a resolution of 0.01 nm and 0.004 nm measurement step. [4; 10; 46]

Reflectivity measurements differ from optical spectrum measurements quite a bit, though having the same principle using monochromator and photodiode. For the reflectivity measurements commercial Perkin Elmer Lambda 1050 was used. In this system output of a white light source, tungsten lamp, is guided through monochromator which is then split 50/50 to two monochromatic beams. One of these beams is reflected from sample and thus by comparing reflected and reference beams absolute reflectivity can be measured directly. In these measurements wavelength accuracy was better than 0.3 nm with 0.2 nm resolution and reflectivity accuracy of better than 0.5 %. [31]

5.3 Beam characterization

Third output character of lasers is brightness which on other words can be expressed in terms of beam quality. Transversal beam profile can be measured with a CCD camera or pyrocamera. In CCD cameras the wavelength range is limited and thus in this thesis the 2.5 μm laser beam is characterized with a Spiricon pyrocam III, PYIII-C-B. Such camera can measure the transversal beam profile and beam diameter, with a pixel size of a 100 μm. [17]

Beam profile can provide information about symmetry and shape of the beam but does not necessarily reveal higher order modes. Thus M2 measurements are needed

to give a practical and reliable value for the beam quality. According to equation (2.15) this can be done by measuring beam diameter with pyrocamera as a function of distance around properly formed waist, described in more detail later.

5.4 Pulse duration measurements using autocorrelation

Autocorrelators (ACs) are devices for measuring the intensity or field autocorrelation function of light, commonly used for determining the duration of ultra-short pulses, where photodiodes are too slow. There are a few types of ACs from which second harmonic intensity autocorrelator is used in this thesis. The principle of operation of such an AC is the following. The pulsed beam is divided into two equal beams with a beam splitter into two delay lines from which the other is variable delay line. These two beams are then non-coaxially superimposed in a nonlinear second harmonic crystal, producing second harmonic signal. The second harmonic signal is thus autocorrelation of the two signals and the average power thus becomes a function of variable temporal delay

$$P_{\mathrm{SHG}}(\tau) \propto \int P(t)P(t+\tau)\mathrm{d}t. \tag{5.1}$$

Advantage of such a method is that power measurement of the second harmonic signal does not require fast photodiode. [16]

The autocorrelation function $P_{\mathrm{SHG}}(\tau)$ in equation (5.1) is depended on the initial pulse shape $P(t)$. Gaussian and hyperbolic secant functions are most often used to describe the pulses. For hyperbolic secant function

$$P(t) \propto \mathrm{sech}^2(t/w), \tag{5.2}$$

the shape of the autocorrelation is also hyperbolic secant, and the pulse duration is 0.648 times the width of the AC trace. Furthermore, the width of the AC trace is 1.7627 times of the width parameter w.[16] In this thesis commercial Femtochrome FR-103XL rapid scanning autocorrelator was used for pulse measurements. It has a resolution of 1 fs [16]. However, as the AC signal was measured with a fast oscilloscope and the pulse width was determined from the fitting result of the function (5.2), the accuracy of pulse durations is limited to fitting accuracy. Accuracy of the fitting was better than 1 %.

6. EXPERIMENTS AND RESULTS

In this chapter, experiments and the results are described in detail. Discussions of the results along with some contrastive data are presented as well.

6.1 Experiments of 2.5 μm semiconductor disk laser

The 2.5 μm semiconductor structure was grown using a solid-source molecular beam epitaxy on an n-GaSb wafer (100) in a single epitaxy run. Elemental indium, aluminum and gallium together with As_4 and Sb_4 were used as group III and V sources respectively. The group V constituents were cracked into As_2 and Sb_2 using high temperature cracking tubes. More detailed growth parameters are described in [28; 26], and the structure parameters in appendix A.

The structure consists of 21.5 pairs of GaSb/AlAsSb DBR and a gain section with 15 $In_{0.35}GaAsSb$ quantum-wells (QWs) surrounded by 20 nm thick $Al_{0.35}GaAsSb$ barriers. The 9.5 nm thick QWs were arranged in groups of three and embedded in $Al_{0.5}GaAsSb$ spacer layers which provides the dominant pump absorption. The gain structure was closed with a lattice-matched AlAsSb window layer to ensure good carrier confinement covered by a thin GaSb cap layer preventing oxidation. Layer thicknesses were selected to form a 3λ micro-cavity between the DBR and the AlAsSb-window with QW groups located at the antinodes of the standing-wave optical field, see figure 3.1. The reflection spectrum of the gain mirror, shown in figure 6.7, reveals the bandwidth of 300 nm owing to the high index contrast of the GaSb/AlAsSb pairs. This characteristic is particularly suitable for wide spectral tuning and short pulse generation.

With 980 nm pumping available for this study, considerable fraction of pump power is contributed to heat generation in the gain element owing to large quantum defect. The intracavity heat spreader technique was applied here as a method which provides efficient heat removal from the gain chip. A 2.5 mm by 2.5 mm size gain chip was capillary bonded with water to a type IIa natural diamond heat spreader to enable efficient heat removal from the active region. The bonded chip was finally sandwiched between two copper plates, with a hole in the top plate allowing the

passage of pump and signal. The mounted sample was attached to a water cooled copper heat sink.

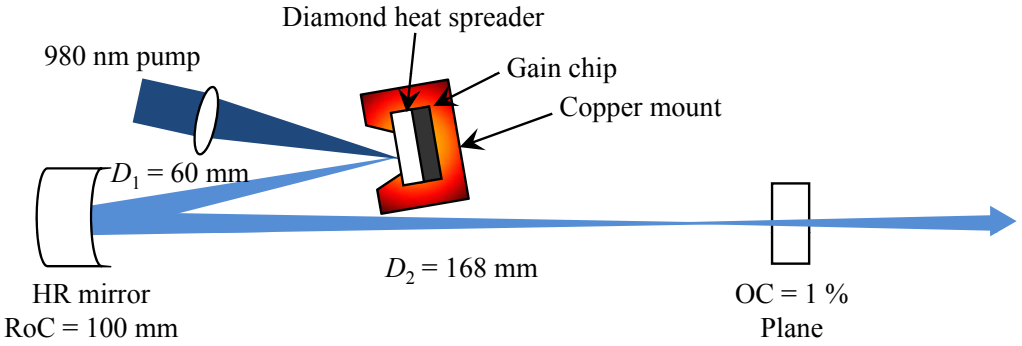

Figure 6.1: Shematic presentation of the V-cavity

For the power scaling and beam quality studies the laser was arranged in a V-shaped cavity as shown in figure 6.1. It was comprised of mounted gain chip, a highly reflective folding mirror and a 1 % plane output coupler. The pump beam from 980 nm fiber coupled diode laser was focused on the gain mirror to a spot of 180 μm diameter at an angle of 30 ° to the surface normal. The cavity was simulated to match the cavity mode size with the pump spot. Commercial *Winlase*-program, that utilizes the equations described in chapter 2.3, was used for these numerical simulations. Stable and suitable solution was found with 100 mm folding mirror curvature and with arm lengths of $D_1 = 60$ mm and $D_2 = 168$ mm, as shown in figure 6.1.

For the M2 measurements a proper beam waist was needed. Large enough beam diameter to be measured with pyrocamera and long focusing distance to enable enough measurements points around the waist. This was obtained by first collimating the output beam with a 1000 mm lens and then focusing it with another 1000 mm lens. Around 50 $1/e^2$ widths was then measured around the waist to fit equation (2.15) into the data.

Spectral tuning studies were repeated in the same cavity as previous experiment. Only with the exception that a 25 μm thick etalon was placed into the longer arm of the cavity. By tilting the etalon, optical length changes as a function of angle θ so that $L = nd\cos(\theta)$, where n is the refractive index and d is the physical thickness of the etalon. As a results, the transmission wavelengths of the etalon changes as well.

6.2 Results of 2.5 μm semiconductor disk laser

In this section all results along with discussions are described. For convenience, the section is divided into two subsections of the two distinct experiments of power scaling and tuning.

6.2.1 Power scaling and beam quality

Output power was measured as a function of pump power at mount temperatures of 5, 10 and 15 °C. Pump reflection loss from the sample was also measured and absorbed pump power was calculated as pump power minus reflection loss. Output powers versus absorbed pump power are shown in figure 6.2. Maximum output power of about 600 mW was achieved at mount temperature of 5 °C, and is clearly limited by the thermal rollover at high power. The power was finally limited to critical power drop or even to a nonoperational state caused by higher losses than the gain. Threshold pump power as absorbed power was 1.52 W for temperature range 5–15 °C, as seen from figure 6.2. The maximum mount temperature for lasing to occur was also tested and it was found to be 40 °C.

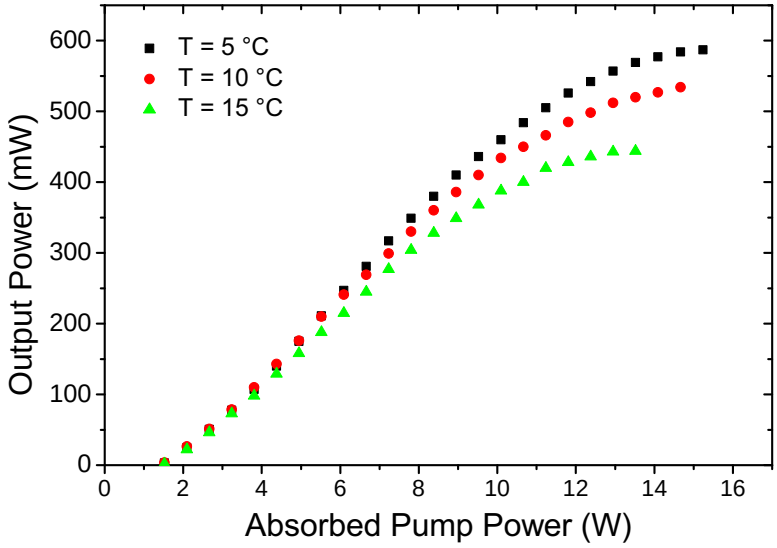

Figure 6.2: Output power at various temperatures

A typical output spectrum is shown in figure 6.3. The individual peaks of the spectrum are due to Fabry–Pérot effect induced by the intra cavity diamond. Wavelength difference of two adjacent fringe is 4.14 nm, and the equation 2.21 gives thickness of 309 μm which corresponds to the physical thickness of the diamond. Refractive index of the diamond is 2.38. A wavelength shift as function of pump

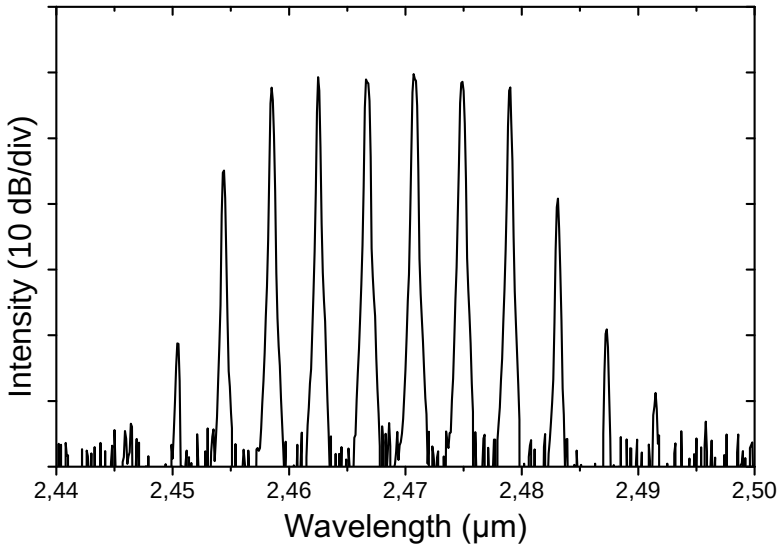

Figure 6.3: Typical spectrum of the 2.5 μm semicondustor disk laser, showing etalon effect of the intra cavity diamond

power was also observed. This tuning from 2.45 μm to beyond 2.5 μm is due to heating of the gain.

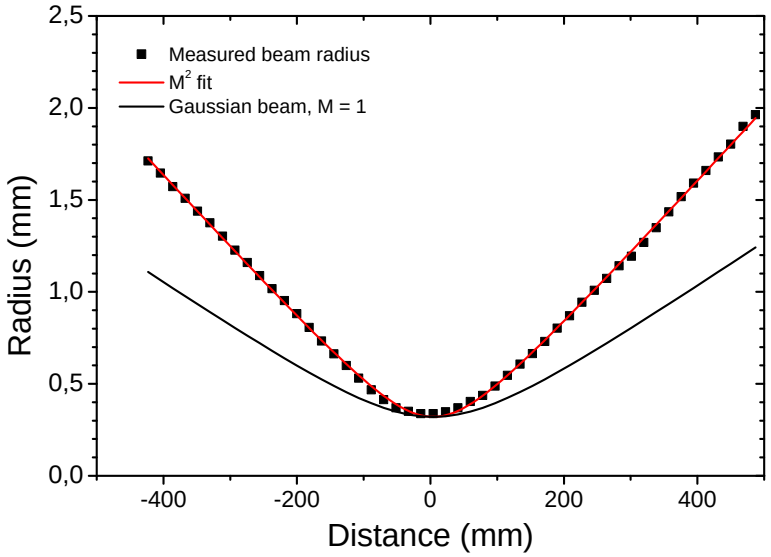

Figure 6.4: Typical M^2 measurement

Figure 6.4 shows a typical M^2 measurement along with fitted and theoretical curves. M^2 values were measured in three different temperatures and at four power level. These are shown in figure 6.5, which clearly shows linear increase in M^2 as function of pump power remaining below 1.6 in all cases. It was also found to be independent of the mount temperature. The beam profile shown in figure 6.5 inset is slightly elliptical due to small angle in the V-cavity.

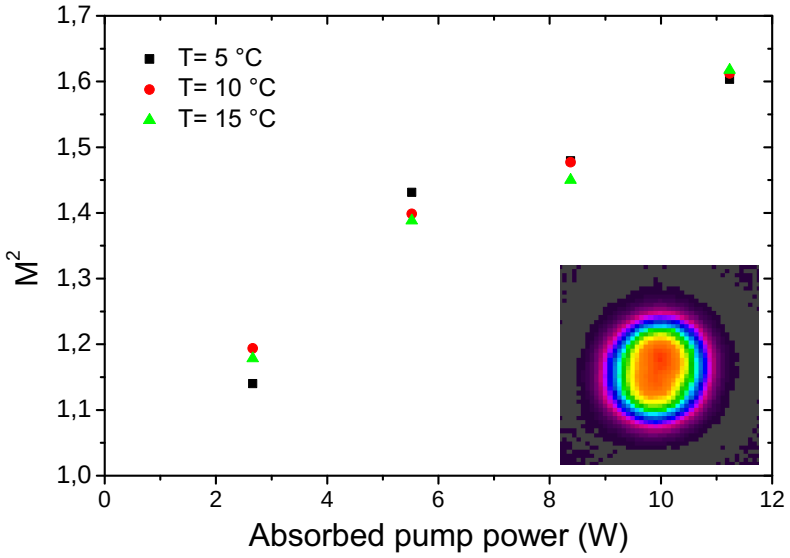

Figure 6.5: M^2-values versus 980 nm absorbed pump power at various temperatures and typical beam profile as an inset.

6.2.2 Tuning results

By tilting the etalon, a total of 130 nm tuning range from 2.414 μm to 2.536 μm was achieved. Maximum power of 308 mW was observed at wavelength of 2.481 μm. Figure 6.6 shows measured spectra normalized to output power, and 6.7 shows the reflectivity curve of the gain mirror, with 300 nm stop-band indicating that is not limiting the tunability. This clearly indicates the usefulness of GaSb-based materials at long wavelengths.

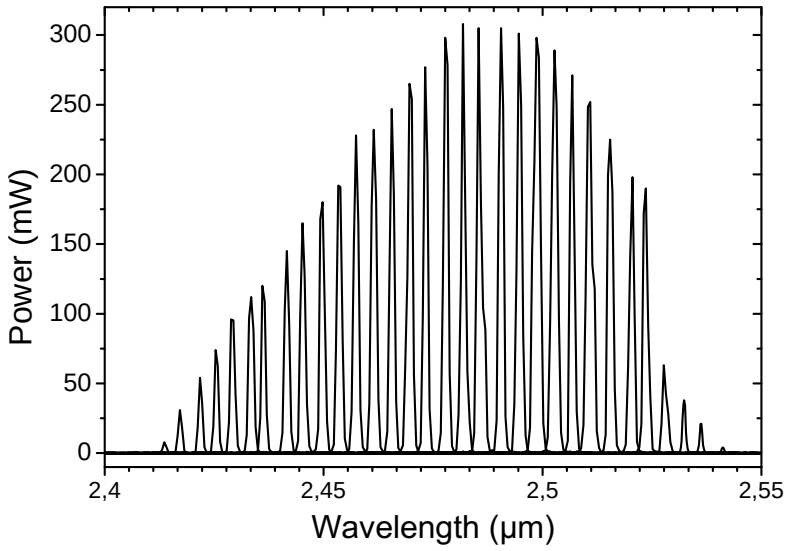

Figure 6.6: Tuning spectra

The 25 μm thick quartz etalon used in this work has 87 nm free spectral range,

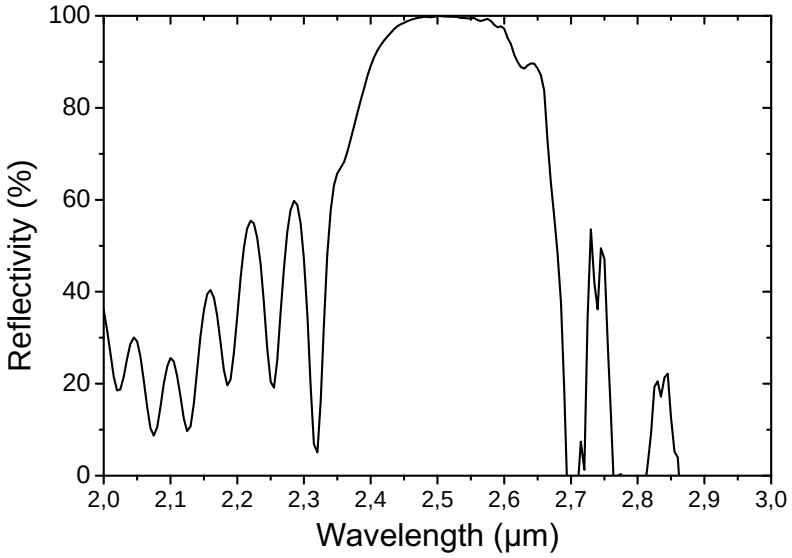

Figure 6.7: Reflectivity of the gain mirror.

as derived from equation (2.21) with refractive index of 1.45. However, the spectral tuning range of a laser is not limited to this range since laser operates at the wavelength were gain is highest and cavity losses smallest. As previous CW measurements showed the gain shifts to longer wavelengths at higher pump power, the pump power was slightly reduced for the few first peaks in order to maintain larger gain on the shorter wavelengths. On the longer wavelengths instead, the mount temperature was increased in order to move gain to the longer wavelengths. This can be seen in the figure 6.6. as a significantly reduced output power for the last three spectra. As a conclusion the tuning range is limited by the free spectral range of the etalon. Furthermore, quartz has losses at 2.5 μm, and thus, the tuning range and power level could be further extended by using low-loss tunable filter.

6.3 Experiments of mode-locked edge-emitting laser

The edge-emitting diode lasers used in this thesis are commercial lasers made by Innolume GmbH. The quantum dot semiconductor structures used in these lasers were grown by a solid-source molecular beam epitaxy on a GaAs wafer. The active regions are comprised of 5 layers of InAs QDs. The lasers are two-section diode lasers with 300 μm long saturable absorbers located near the back facets. These two laser diodes operate at 1.2 μm and 1.3 μm wavelength and their total lengths are 1.3 mm and 4.0 mm, respectively. The front and back facets are anti-reflection $\sim$3 % and high-reflection $\sim$95 % coated, respectively.

Both diode lasers are soldered to a sub-mount for wire bonding which in addition

works as anode contact. The sub-mount is further soldered to a copper-mount which also serves as a heat sink and thus the mounted sample is attached to peltier cooled stage. Temperature was monitored with an AD590 temperature sensor and the cooling was controlled by a PID controlled peltier. Forward bias was current controlled by laser diode driver and backward bias for absorber was supplied from separate voltage supply.

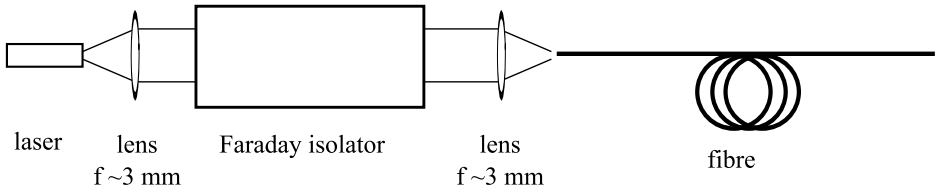

Figure 6.8: Schematic presentation of the measurement setup used to characterize edge-emitting lasers.

For the laser characterization and Bi-fiber studies the laser light was launch into a fiber with a simple two lens setup as shown in figure 6.8. Highly divergent output beam of the edge-emitting diode lasers were first collimated with a spherical high numerical aperture lens with focal length of 3.1 m and NA of 0.68. The collimated beam was finally focused into a single-mode fiber with a similar lens. In order to avoid feedback into the laser from such optical system, a Faraday isolator was placed between the lenses. Moreover, lenses were mounted on 3-axis translational stages with micrometers allowing fine positioning of the lenses in both transverse and longitudinal aligning. The final aligning of the system was done by positioning the lenses for the maximum output power at the end of the fiber.

In the laser characterization studies the power was measured with an integrating sphere detector directly after the first collimating lens before the isolator. Spectra and pulses were however measured from the fiber output as required by the measurement devices. In the Bi-fiber studies this setup was simply spliced to a Bi-fiber setup, shown in figure 6.16 and thus such setup is considered as a single signal laser.

6.4 Results of mode-locked edge-emitting laser

Output power of 1.2 μm diode laser was measured as a function of current and backward absorber bias voltage at mount temperature of 20 °C. Measured power values are shown in table 6.1 and the corresponding plot is shown selectively from the shortest pulses in figure 6.9 a. Autocorrelation was also measured in each current & bias setting and the pulse widths derived from secant fittings described in section 5.4 are shown in table 6.2 and figure 6.9 b. Corresponding peak power is calculated

with repetition rate 30.45 GHz from laser specifications and are shown in table 6.3 and figure 6.9 c. From figure 6.9 b it is clear that the output power is linear versus pump current for constant bias. It is also clear that the power is reduced when absorber bias is increased while pulses are also shortened.

Table 6.1: Average power (mW) of the 1.2 μm laser diode measured after collimation lens

		Bias (V)							
		1	1.5	2	2.25	2.5	2.75	3	3.5
Current (mA)	300	49.5	46.4	44.0		38.2		33.8	32.1
	325			53.6	49.8	46.8	45.8	44.1	
	350	76.7	70.6	63.4	58.3	55.3	54.6	52.6	50.2
	375			70.7	63.6	61.0	60.4	58.1	
	400			78.6	71.0	68.7	67.4	65.0	61.0
	428					73.6			
	433				79.0				

Table 6.2: Pulse widths (ps) of the 1.2 μm laser diode. (Hyperpolic secant fit)

		Bias (V)							
		1	1.5	2	2.25	2.5	2.75	3	3.5
Current (mA)	300	9.07	8.42	7.38		6.04		6.79	8.64
	325			5.74	5.14	5.49	5.86	5.77	
	350	8.85	8.01	5.64	5.57	5.73	5.93	6.11	8.15
	375			6.07	5.31	5.59	5.92	5.83	
	400			6.30	5.56	6.10	6.28	6.23	8.37
	428					7.16			
	433				6.10				

Typical autocorrelation traces are shown in figures 6.10 and 6.11 where 6.10 reveals 6 autocorrelation peaks due to high ∼30 GHz repetition rate and 6.11 shows a typical single peak with fitted hyperbolic secant function. Moreover, the traces indicates stable mode locking which is seen as uniform AC trace over the scan in figure 6.10, and low noise which is seen figure 6.11 as smooth data and excellent fit. Furthermore, a typical spectrum is shown in figure 6.12. Peaks in the spectrum are caused by the short Fabry–Pérot cavity of the laser, which also corresponds to the repetition rate.

The motivation of these studies was to do detailed analysis at laser output characteristics for master oscillator power amplifier (MOPA), edge-emitting laser diodes are master oscillators and Bi-fiber as power amplifier. This motivation sets a few targets and requirements for the output characteristics. First of all, the wavelength must be close to the emission spectrum of the Bi-fiber, which is around 1.18 μm in

Table 6.3: Peak power (mW) of the 1.2 μm laser diode. Calculated from average power and pulse widths with 30.45 GHz repetition rate.

		Bias (V)							
		1	1.5	2	2.25	2.5	2.75	3	3.5
Current (mA)	300	158	159	172		183		144	108
	325			270	281	247	226	221	
	350	251	255	325	303	279	266	249	178
	375			337	346	316	295	289	
	400			361	369	326	310	302	211
	428					297			
	433				375				

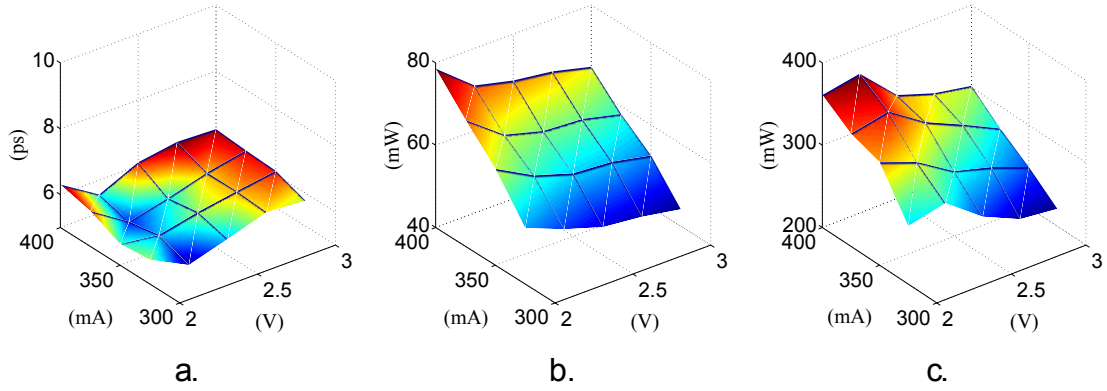

Figure 6.9: Results of 1.18 μm laser. a. Pulse duratiob, b. average power, and c. peak power as a function of pump current and reverse bias voltage.

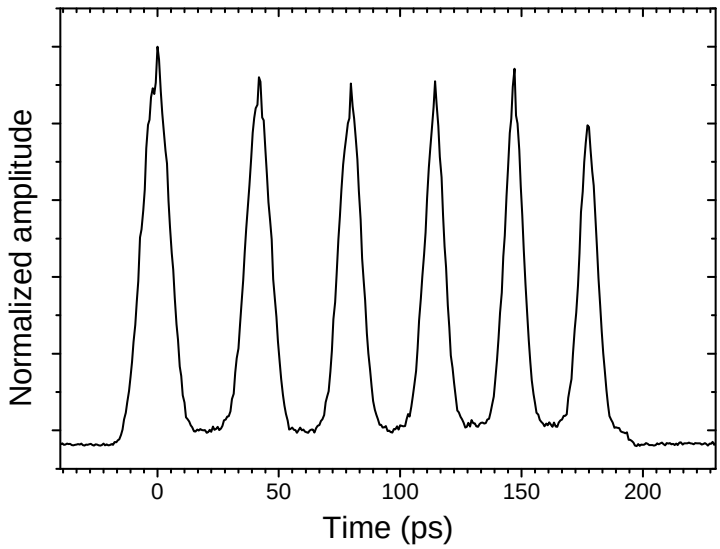

Figure 6.10: Full scanning scale AC trace showing multiple AC peaks due to high repetition rate

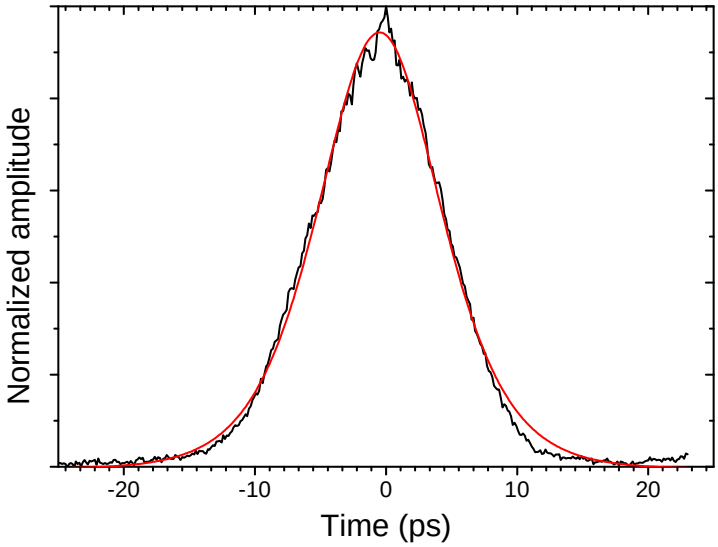

Figure 6.11: Single AC trace with hyperbolic secant fit

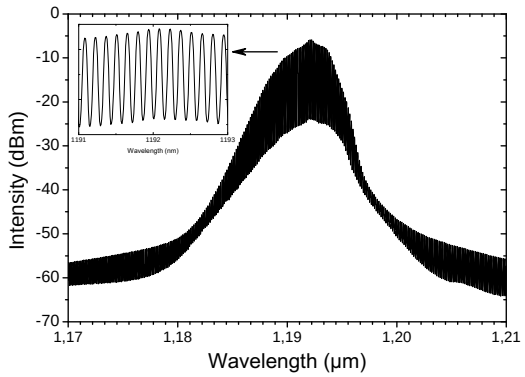

Figure 6.12: Typical spectrum. Longitudinal modes are shown in detail in inset.

this case. As it was discussed previously that QD laser can lase at two wavelengths simultaneously: from excited state as well as from ground state independently. This sets limitations to the current and bias values in order to keep the lasing from ground state as it was found to be the origin of 1.2 μm lasing. The measurements shown here are thus only from 1.2 μm lasing. However, a lot higher powers and shorter pulses were observed at excited state mode-locking at shorter wavelength, but are disregarded within this thesis due to wavelength requirements set by the Bi-fibers.

The output characteristics were tried to be improved by adjusting the temperature and thus the diode laser was tested also in lower and higher temperatures than 20 °C. However, increasing temperature resulted in remarkable power loss in addition to the already low average power of less than 71 mW limited by wavelength limitation, and thus temperature increase was out of the question. On the other hand decreasing the temperature allowed excited state lasing to occur at lower currents which resulted in further limitations on pumping and average output power. These observations were done with 10–15 °C differences from the original 20 °C temperature set, and thus the normal room temperature of 20 °C was used throughout these studies.

From the point of telecommunication, short pulses with modest average power, and highest peak powers, are most desirable also for this study. Under these and previous considerations it can be stated from figure 6.9 that the optimum performance of the laser in these studies is at forward current of 400 mA and absorber reverse bias of 2.25 V, resulting in 71 mW of output power with 5.56 ps pulse width. From table 6.1 can be seen that this is not an ultimate power limit for laser to operate at 1.2 μm. However, bistable operation between ground state and excited state lasing was observed above 400 mA current levels and thus it is more convenient to operate at stable 400 mA currents.

Both of the diode lasers, used in this thesis, are similar to each other by their design and behavior. The only differences occur in physical length, wavelength and in output characteristics. Thus the 1.3 μm diode laser was tested in similar way and the results shown here are selected from those where the lasing wavelength remains at 1.3 μm region required by another Bi-fiber. The 1.3 μm diode laser was also tested at mount temperature of 20 °C and the corresponding results are shown in tables 6.4–6.6 and figures 6.13 and 6.15.

A typical autocorrelation trace is shown in figure 6.14 with fitted hyperbolic secant function. Excellent fit of the AC trace indicates undistorted and pure mode-locking. The slightly higher noise compared to the 1.2 μm diode laser arises simply

Table 6.4: Average power (mW) of the 1.3 μm laser diode measured after collimation lens

	Bias (V)				
	4.5	5.0	5.5	6.0	6.5
Current (mA) 250	14.1	13.2	11.2	(12.5)[1]	(11.5)[1]
275	18.8	17.5	16.4	15.6	(14.5)[1]
300	23.8	22.3	20.4	19.8	(17.9)[1]
310	25.7	24.2	22.0	21.5	(19.7)[1]

[1] Laser operates at 1.24 μm. (ES ML)

Table 6.5: Pulse widths (ps) of the 1.3 μm laser diode. (Hyperpolic secant fit)

	Bias (V)				
	4.5	5.0	5.5	6.0	6.5
Current (mA) 250	9.9	6.1	5.2	(4.7)[1]	(4.6)[1]
275	12.7	8.5	6.3	5.5	(4.9)[1]
300	18.5	12.6	8.3	6.5	(6.0)[1]
310	21.5	15.1	8.3	7.6	(6.4)[1]

[1] Laser operates at 1.24 μm. (ES ML)

Table 6.6: Peak power (mW) of the 1.3 μm laser diode. Calculated from average power and pulse widths with 10.2 GHz repetition rate.

	Bias (V)				
	4.5	5.0	5.5	6.0	6.5
Current (mA) 250	123	187	186	(230)[1]	(216)[1]
275	128	178	225	245	(255)[1]
300	111	153	212	263	(258)[1]
310	103	138	229	244	(266)[1]

[1] Laser operates at 1.24 μm. (ES ML)

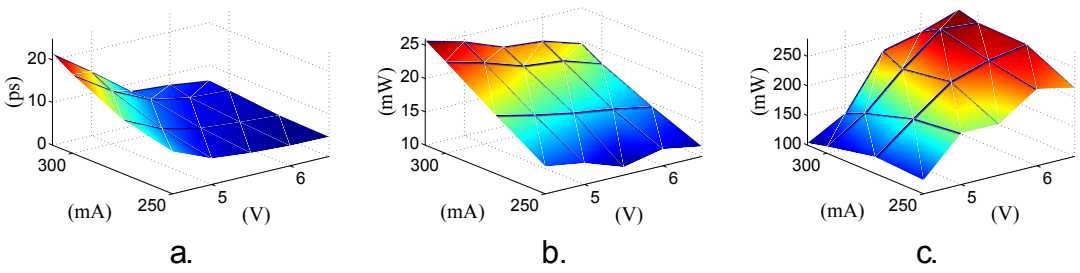

Figure 6.13: Results of 1.29 μm laser. a. Pulse duration, b. average power, and c. peak power as a function of pump current and reverse bias voltage.

from the need of electrical amplification of the AC measurement due to low output power. Furthermore, a typical spectrum is shown in figure 6.15. Fringes in the spectrum are caused by the Fabry–Pérot cavity of the diode laser, which also corresponds to the repetition rate of 10.2 GHz.

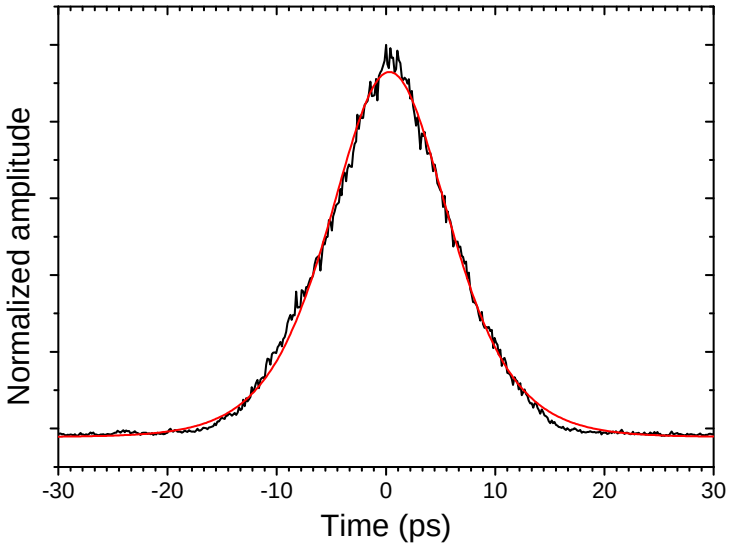

Figure 6.14: Single AC trace with hyperbolic secant fit

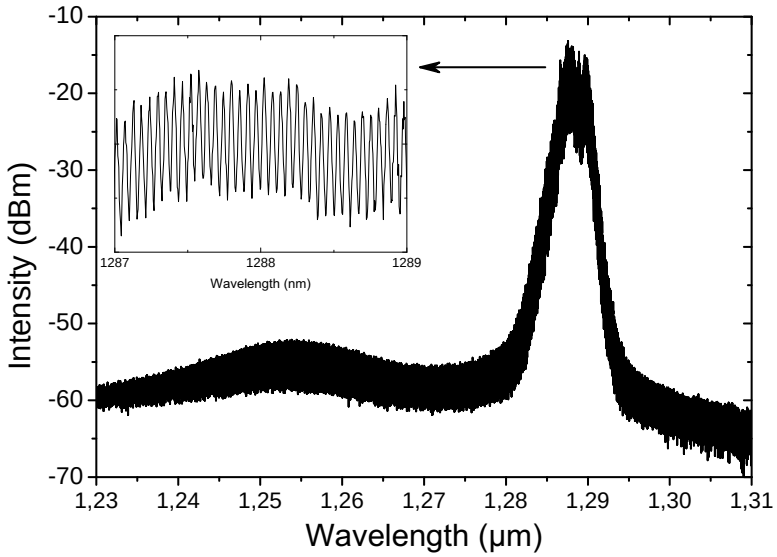

Figure 6.15: Typical spectrum. Fringes are shown in detail in inset

The motivation here was also to do detailed analysis of the output characteristics in order to be used as a signal laser for the Bi-doped fiber amplifier. However, in this case the desired wavelength is around 1.3 μm. In a similar way the lasing from ground state was found to be the origin of 1.3 μm lasing. This sets even more limited operating values for pump current and absorber bias in order to keep the

lasing at 1.3 μm. Thus the maximum average power at this wavelength was limited to only 26 mW, while the average power of excited state lasing was in the range of hundreds of mW. These measurements are as well disregarded within this thesis due to wavelength requirements.

The output characteristics were also attempted to improve with this 1.3 μm diode laser sample by adjusting the temperature. In this case, increased temperature resulted in critical power loss in addition to the already poor average power of less than 26 mW. On the other hand, in this case, decreasing the temperature allowed increased pump currents and thus slightly higher powers from ground state lasing. However, decreased temperature shifted spectrum to shorter wavelengths away from the optimum 1.3 μm of the 2nd Bi-fiber. It is seen in figure 6.15 that the output spectrum was already centered at 1.289 μm and thus the temperature of 20 °C was found to be convenient for these studies.

According to figure 6.13 and tables 6.4–6.6, for 1.3 μm diode laser, the optimum performance of the laser was found to be at forward current of 300 mA and absorber reverse bias of 5.5 V, resulting in 20.4 mW of output power with 8.3 ps pulse duration. Also in this case, bistable operation was observed and thus the pumping was limited to 300 mA current.

6.5 Experiments with Bi-amplifier results

The fibers in this work were made using surface-plasma chemical vapor deposition (SPCVD) technology which is quite new method for Bi-fibers. However, it has been used previously for Er-doped fibers. [1; 30]. These experiments are not a subject of this thesis but are however related to the edge-emitting laser experiments. The main points and results of MOPA studies are discussed here in order to emphasize the requirements for the edge-emitting lasers. The type of fibers used in this study are described in more detail in [1].

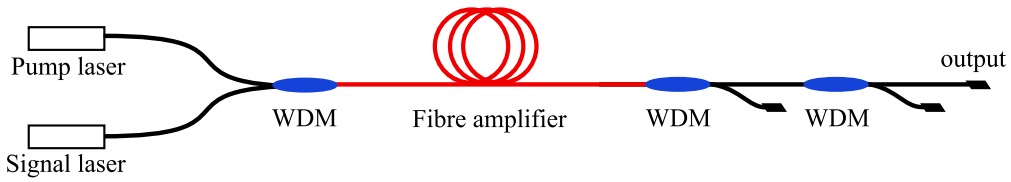

Figure 6.16: Shematic presentation of the Bi-doped fiber amplifier setup.

The setup of Bi-fiber amplifier is shown in figure 6.16. In both cases the pump laser and the signal laser are connected to the active fiber via wavelength-division

multiplexer (WDM) and after the active fiber residual pump is filtered out by other two WDMs. In the 1.2 μm Bi-fiber studies a 1060 nm Yb-doped fiber lasers were used as a pump source and in the 1.3 μm case a 1.22 μm QD-based OP-SDL was used.

6.6 Results of Bi-fiber amplifier

Output power and characteristics were measured only with the highest pump power of 690 mW and the maximum signal laser average power provided into fiber was only 10 mW. The signal was operated at the optimal performance point of -2.25 V reverse bias and 400 mA current providing total 71 mW of average power. It is now seen that the total loss of the fiber connection exceeds 8.5 dB caused mainly by the poor beam quality of the signal laser but also the WDM losses. Input pulse width is 5.8 ps and the center of the spectrum is at 1.19 μm with spectrum width of roughly 3.3 nm.

The measurements were first made with 18 m long active fiber on at two ambient temperatures 300 K and 77 K. The unabsorbed pump power equaled 13.6 mW at 300 K and 126.3 mW at 77 K. The liquid nitrogen at 77 K was used to minimize acoustic vibration of the crystal lattice and increase amplification. The ASE sources and spectra of Bi-doped fiber amplifier are presented in figures 6.17 and 6.18.

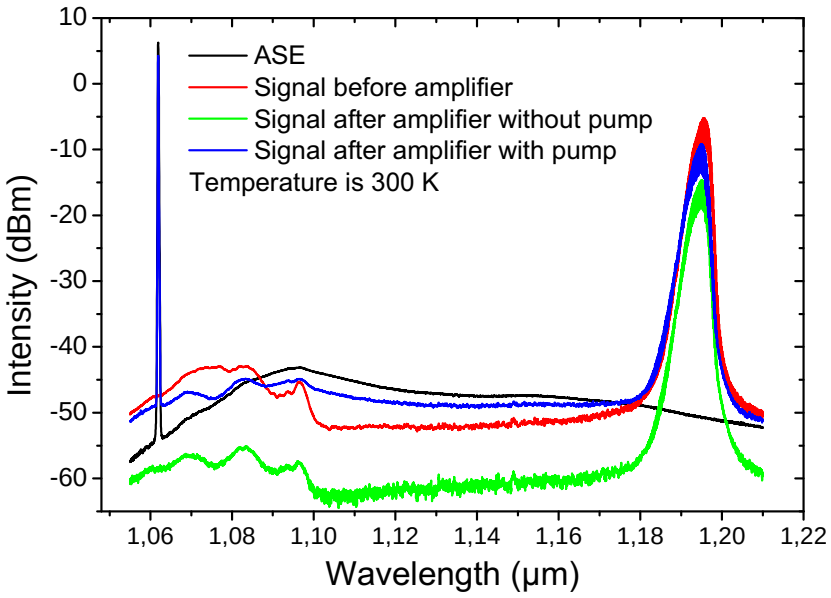

Figure 6.17: Spectra of 18 m long amplifier at temperatures of 300 K.

The operation of Bi-doped fiber laser was observed at 300 K and 77 K. The amplification was achieved at 77 K and equaled of 4.8 dB i.e. 0.27 dB/m. The

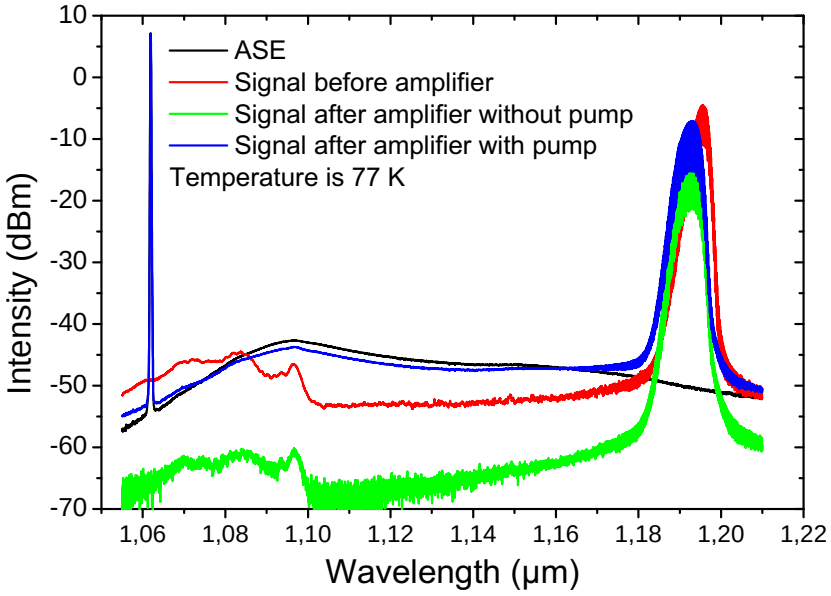

Figure 6.18: Spectra of 18 m long amplifier at temperatures of 77 K.

output power of amplified signal was measured using two WDMs for residual pump filtering and amounted to 30 mW, whereas at room temperature it was 12 mW. As the amount of residual pump was fairly high and amplification low the amplifier was then extended to 24 m.

With 24 m long amplifier the unabsorbed pump power equaled 2.72 mW at 300 K and 47 mW at 77 K. Output powers, including unabsorbed pump power, were 17.7 mW at 300 K and 96.6 mW at 77 K. Input signal power into fiber was the same 10.9 mW. Thus, a total of 6.6 dB of amplification was achieved.

The pulse widths of the amplified signals were also measured at each temperature and length of active fiber and the corresponding autocorrelation traces are shown in figures 6.19 and 6.20. The pulse durations were broadened to around 7.1 ps from the input of 5.8 ps due to dispersion of the silica fiber. Furthermore, due to measurement accuracy, difference between 18 m and 24 m long amplifiers was not observed. Also, as expected, temperature does not have measurable effect to the pulse broadening.

The 1.3 μm Bi-fiber amplifier studies resulted in very poor results. Only a fraction from several hundreds of mW of pump power was absorberd by active fiber and thus the amplification was very low. Only 12.6 mW output power was achieved from 6.6 mW input power to the active fiber, meaning 2.8 dB of total amplification and less than 0.1 dB/m of amplification. Such a result is lot less than was expected and desired and thus there was no point continuing the measurements.

In order to continue this research both signal laser and Bi-fiber should be improved. Especially the amount of signal laser power launch into active fiber must be

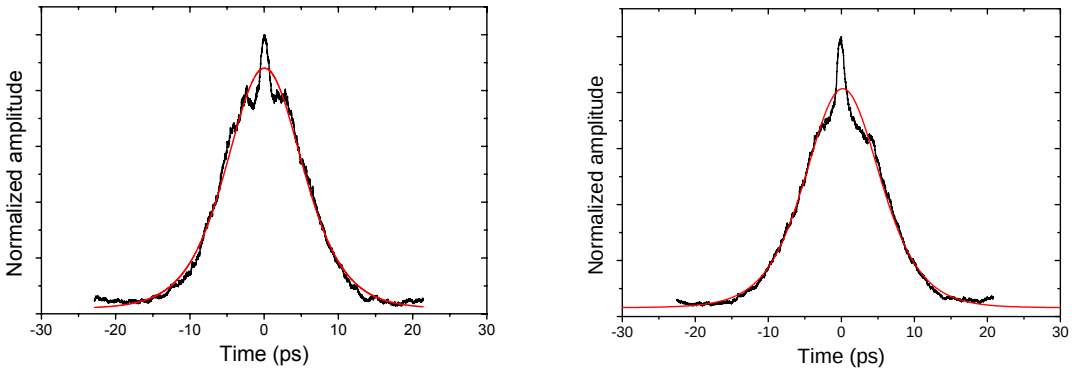

a. b.

Figure 6.19: Autocorrelations of 18 m long amplifier at temperatures of a. 300 K, and b. 77 K. Some chirping can be seen as peak in top AC-traces.

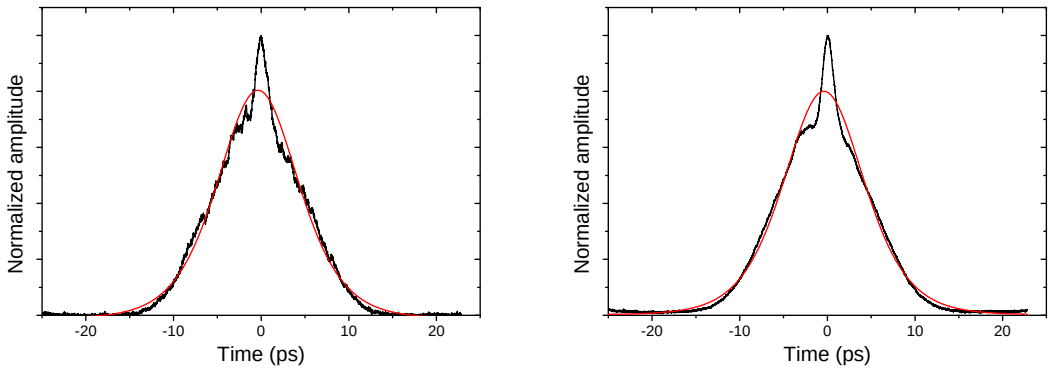

a. b.

Figure 6.20: Autocorrelations of 24 m long amplifier at temperatures of a. 300 K, and b. 77 K. Some chirping can be seen as peak in top AC-traces.

increased. This could be first done by using more suitable signal laser with higher power, but also by minimizing the losses at WDM and in the fiber connection of the signal laser.

It was found that the highest loss of signal laser power was from fiber connection due to rather poor and highly elliptical beam of the edge-emitting laser. This could be improved by using more sophisticated collimation and focusing system. Especially the output beam of the edge-emitting lasers could be shaped into circular beam using two cylindrical lenses for fast- and slow-axis separately. However, such a setup would increase the complexity and thus the functionality of the system. The overall cost of the setup would increase as well.

7. CONCLUSIONS AND FUTURE WORK

For the first time [28; 26], a GaSb-based OP-SDL operating at 2.5 μm spectral range has been demonstrated operating in the continuous wave as well as tunable laser. Moreover, fabrication and characterization of GaSb-based SDLs have been presented. With an intra-cavity diamond heat spreader for thermal management, 600 mW of continuous wave output power with good beam quality has been achieved. Tunable operation of 130 nm with output power up to 310 mW has been obtained limited by the free spectral range and loss induced by the etalon.

In comparison to other results given to date, over 4 W at 2 μm [11; 43] has been achieved. Extended to longer wavelengths 0.6 W at 2.33 μm [37] and over 2 W at 2.35 μm as in-well pumped [38] has also been achieved. And a year after the results achieved in this thesis, 120 mW at 2.8 μm [35] was reported. In respect to these reports it is seen how much harder it is to achieve high powers when wavelength is extended from 2 to 3 μm, and thus the 600 mW and 130 nm tuning achieved in this thesis are remarkably good results. As for tuning only tunability of about 25 nm at 2.3 μm [15] has been reported.

As a conclusion the results show that the advantages of high-power disk laser technology can be extended to 2.5 μm and beyond utilizing (AlGaIn)(AsSb) semiconductor compounds. Moreover, such material system was found to provide both wide band low loss mirrors and wide gain desired for tunable lasers. Last but not least, high power and high brightness was achieved as expected.

Higher power and better beam quality was found to be limited by substantial thermal load on the SDL. Further improvement in power scaling could, therefore, be expected with implementation of optical pumping at longer wavelength. Particularly commercially available erbium-based lasers operating at 1.55 μm should give 38 % lower quantum defect. Another option could be in-well pumping with a 2 micron diode laser source. Beam degradation due to thermal lens as well as wider tunability could be also improved due to lower thermal load. Added to this, implementing low-loss filter with large tuning range could also improve tunability.

In the second part of the thesis, mode-locked edge-emitting quantum-dot lasers operating at 1.2 μm and 1.3 μm spectral range has been characterized in detail to

meet the requirements as seed laser for Bi-fiber amplifier. For the 1.2 μm laser diode the optimum performance resulted in 71 mW of average output power for 5.56 ps pulses with the repetition rate of 30.45 GHz. Respectively, for 1.3 μm laser diode it was 20.4 mW of average output power for 8.3 ps pulses at 10.2 GHz repetition rate. For both diode lasers the stable mode-locking was found to associate from the ground state lasing. As for the Bi-fiber amplifiers, only 0.274 dB/m and 0.1 dB/m amplification was achieved at 1.2 μm and 1.3 μm respectively. Moreover pulse widths were broadened few picoseconds due to dispersion in the fibers.

As a conclusion it is shown that mode-locked edge-emitting lasers can be used as a compact ultrafast seed signal source for Bi-fiber amplifiers. Fiber amplifier results on the other hand were rather poor due to a lack of efficient amplifier fibers. First of all simple collimating-focusing system was used which resulted in significant loss of power when multimode output of laser diode was coupled into single mode fiber. Secondly, due to wavelength matching laser diodes had to be operated at ground state mode-locking whilst exited state mode-locking could give hundreds of milliwatts directly. Thirdly, amplification of Bi-fibers was none the less rather weak due to losses in fibers caused by acoustic vibrations of the crystal lattices. As an example for comparison amplification in typical erbium amplifiers could be several dBs per meter [7].

Future work based on conclusions should first concentrate on matching the wavelength of exited state mode-locking to Bi-fibers wavelengths and thus full power capacity of laser diode could be used. Secondly, the fiber coupling should be replaced by separated fast- and slow-axis collimation lenses. Furthermore, the performance of bismuth-doped fiber amplifier is expected to be improved in the near future, which would have a promising impact on the telecom technology.

BIBLIOGRAPHY

[1] Igor A. Bufetov, Konstantin M. Golant, Sergey V. Firstov, Artem V. Kholodkov, Alexey V. Shubin, and Evgeny M. Dianov. Bismuth activated alumosilicate optical fibers fabricated by surface-plasma chemical vapor deposition technology. *Appl. Opt.*, 47(27):4940–4944, Sep 2008.

[2] Maria Ana Cataluna, Daniil I. Nikitichev, Spiros Mikroulis, Hercules Simos, Christos Simos, Charis Mesaritakis, Dimitris Syvridis, Igor Krestnikov, Daniil Livshits, and Edik U. Rafailov. Dual-wavelength mode-locked quantum-dot laser, via ground and excited state transitions: experimental and theoretical investigation. *Opt. Express*, 18(12):12832–12838, Jun 2010.

[3] ILX Lightwave Corporation. *User's Guide, InGaAs Power Head OMH-6708B.*

[4] Yokogawa Electric Corporation. *User's Manual, AQ6317C Optical Spectrum Analyzer.*

[5] S.W. Corzine, R.S. Geels, J.W. Scott, R.-H. Yan, and L.A. Coldren. Design of fabry-perot surface-emitting lasers with a periodic gain structure. *Quantum Electronics, IEEE Journal of*, 25(6):1513 –1524, jun 1989.

[6] J.E. Hastie J.-M. Hopkins S. Calvez Chan Wook Jeon D. Burns R. Abram E. Riis A.I. Ferguson M.D. Dawson. Mode-locked quantum-dot lasers. *Photonics Technology Letters*, 15:894 – 896, 2003.

[7] E. Desurvire, J. R. Simpson, and P. C. Becker. High-gain erbium-doped traveling-wave fiber amplifier. *Opt. Lett.*, 12(11):888–890, Nov 1987.

[8] Y. Ding, D.I. Nikitichev, I. Krestnikov, D. Livshits, M.A. Cataluna, and E.U. Rafailov. Quantum-dot external-cavity passively modelocked laser with high peak power and pulse energy. *Electronics Letters*, 46(22):1516 –1518, 28 2010.

[9] A. Garnache, A. Liu, L. Cerutti, and A. Campargue. Intracavity laser absorption spectroscopy with a vertical external cavity surface emitting laser at 2.3μm: Application to water and carbon dioxide. *Chemical Physics Letters*, 416(1-3):22 – 27, 2005.

[10] APE Angewandte Physik & Elektronik GmbH. *Data Sheet, APE Laser Spectrum Analyser.*

[11] M. Guina, A. Härkönen, S. Suomalinen, J. Paajaste, R. Koskinen, M. Pessa, and O. Okhotnikov. Gasb-based compounds tailored for mid-ir disk lasers. *Proc. SPIE*, 7193:71931F–71931F–10, 2009.

[12] A Härkönen, S Suomalainen, E Saarinen, L Orsila, R Koskinen, O Okhotnikov, S Calvez, and M Dawson. 4 w single-transverse mode vecsel utilising intracavity diamond heat spreader. *Electronics Letters*, 42(12):693–694, 2006.

[13] E. Hecht. *Optics*. Addison-Wesley, 2002.

[14] J.-M. Hopkins, S. Calvez, A. J. Kemp, J. E. Hastie, S. A. Smith, A. J. Maclean, D. Burns, and M. D. Dawson. High-power vertical external-cavity surface-emitting lasers. *physica status solidi (c)*, 3(3):380–385, 2006.

[15] J.-M. Hopkins, A.J. Maclean, D. Burns, N. Schulz, M. Rattunde, C. Manz, K. Kohler, and J. Wagner. Tunable, single-frequency, diode-pumped 2.3 μm vecsel. In *Lasers and Electro-Optics, 2006 and 2006 Quantum Electronics and Laser Science Conference. CLEO/QELS 2006. Conference on*, pages 1–2, May 2006.

[16] Femtochrome Research inc. *FR-103XL auto/crosscorrelator, Operation Instructions.*

[17] Ophir-Spiricon Inc. *Operator's manual, Pyrocam III.*

[18] E. Kapon. *Semiconductor Lasers: Fundamentals*. Optics and photonics. Academic Press, 1998.

[19] A.J. Kemp, G.J. Valentine, J.-M. Hopkins, J.E. Hastie, S.A. Smith, S. Calvez, M.D. Dawson, and D. Burns. Thermal management in vertical-external-cavity surface-emitting lasers: finite-element analysis of a heatspreader approach. *Quantum Electronics, IEEE Journal of*, 41(2):148 – 155, feb. 2005.

[20] Alan J. Kemp, Jennifer E. Hastie, Scott A. Smith, John-Mark Hopkins, Stephane Calvez, Gareth J. Valentine, Martin D. Dawson, and David Burns. Heatspreader-based thermal management in vecsels: Thermal lensing in microchip devices. In *Advanced Solid-State Photonics*, page MB34. Optical Society of America, 2005.

[21] Sprague R. Kuznetsov M., Hakimi F. and Mooradian A. Design and characteristics of high-power ($>$ 0.5-w cw) diode-pumped vertical-external-cavity

surface-emitting semiconductor lasers with circular tem00 beams. *Selected Topics in Quantum Electronics, IEEE Journal of*, 5(3):561 –573, may/jun 1999.

[22] Coldren L.A., Corzine S.W., and Mashanovitch M.L. *Diode Lasers and Photonic Integrated Circuits*. Wiley Series in Microwave and Optical Engineering. Wiley, 2012.

[23] Ophir Optronics Ltd. *Ophir Thermal Power Sensors Gatalog.*

[24] A. J. Maclean, R. B. Birch, P. W. Roth, A. J. Kemp, and D. Burns. Limits on efficiency and power scaling in semiconductor disk lasers with diamond heatspreaders. *J. Opt. Soc. Am. B*, 26(12):2228–2236, Dec 2009.

[25] D. Nikitichev, Y. Ding, M. Ruiz, M. Calligaro, N. Michel, M. Krakowski, I. Krestnikov, D. Livshits, M. Cataluna, and E. Rafailov. High-power passively mode-locked tapered inas/gaas quantum-dot lasers. *Applied Physics B: Lasers and Optics*, 103:609–613, 2011. 10.1007/s00340-010-4290-5.

[26] J. Nikkinen, J. Paajaste, R. Koskinen, S. Suomalainen, and O. Okhotnikov. Gasb-based semiconductor disk laser with 130 nm tuning range at 2.5 μm. *Photonics Technology Letters, IEEE*, PP(99):1, 2011.

[27] O.G. Okhotnikov. *Semiconductor Disk Lasers: Physics and Technology*. John Wiley & Sons, 2010.

[28] J. Paajaste, R. Koskinen, J. Nikkinen, S. Suomalainen, and O.G Okhotnikov. Power scalable 2.5 μm (AlGaIn)(AsSb) semiconductor disk laser grown by molecular beam epitaxy. *Journal of Crystal Growth*, 323(71):454 – 456, 2011. Proceedings of the 16th International Conference on Molecular Beam Epitaxy (ICMBE).

[29] R. Paschotta. *Encyclopedia of Laser Physics and Technology*. John Wiley & Sons, 2008.

[30] D. Pavy, M. Moisan, S. Saada, P. Chollet, P. Leprince, and J. Marrec. Fabrication of optical fiber preforms by a new surface-plasma cvd process. *in Proceedings of 12th European Conference on Optical Communications*, pages 19–22, 1986.

[31] 2007. PerkinElmer, Inc. *Technical Specifications for the LAMBDA 1050 UV/Vis/NIR and LAMBDA 950 UV/Vis/NIR Spectrophotometers.*

[32] Diehl R. *High-Power Diode Lasers: Fundamentals, Technology, Applications*. Topics in Applied Physics. Springer, 2000.

[33] Kuznetsov M. Hakimi F. Sprague R. and Mooradian A. Design and characteristics of high-power (>0.5-w cw) diode-pumped vertical-external-cavity surface-emitting semiconductor lasers with circular $tem_0 0$ beams. *Selected Topics in Quantum Electronics*, 5(3):561 – 573, May/Jun 1999.

[34] Sibbett W. Rafailov E. U., Cataluna M. A. Mode-locked quantum-dot lasers. *Nature Photonics*, 1:395 – 401, 2007.

[35] Benno Rösener, Marcel Rattunde, Rüdiger Moser, Sebastian Kaspar, Tino Töpper, Christian Manz, Klaus Köhler, and Joachim Wagner. Continuous-wave room-temperature operation of a 2.8 μm gasb-based semiconductor disk laser. *Opt. Lett.*, 36(3):319–321, Feb 2011.

[36] B.E.A. Saleh and M.C. Teich. *Fundamentals of photonics*. Wiley series in pure and applied optics. Wiley-Interscience, 2007.

[37] N. Schulz, M. Rattunde, C. Manz, K. Kohler, C. Wild, and J. Wagner. High power gasb-based optically pumped vecsel at 2.3 μm. In *Lasers and Electro-Optics, 2006 and 2006 Quantum Electronics and Laser Science Conference. CLEO/QELS 2006. Conference on*, pages 1–2, May 2006.

[38] Nicola Schulz, M. Rattunde, Christian Ritzenthaler, B. Rosener, Christian Manz, K. Kohler, Joachim Wagner, and Uwe Brauch. Resonant optical in-well pumping of an (algain)(assb)-based vertical-external-cavity surface-emitting laser emitting at 2.35 μm. *Applied Physics Letters*, 91(9):091113–091113–3, Aug 2007.

[39] Kyurhee Shim, Herschel Rabitz, and Partha Dutta. Band gap and lattice constant of $ga_x in_{1-x} as_y sb_{1-y}$. *Journal of Applied Physics*, 88(12):7157 –7161, December 2000.

[40] A.E. Siegman. *Lasers*. University Science Books, 1986.

[41] O. Svelto. *Principles of Lasers*. Springer, 2009.

[42] D. Titterton. Development of infrared countermeasure technology and systems. In Anthony Krier, editor, *Mid-infrared Semiconductor Optoelectronics*, volume 118 of *Springer Series in Optical Sciences*, pages 635–671. Springer Berlin, Heidelberg, 2006. 10.1007/1-84628-209-8_20.

[43] Tino Töpper, Marcel Rattunde, Sebastian Kaspar, Rüdiger Moser, Christian Manz, Klaus Köhler, and Joachim Wagner. High-power 2.0 μm semiconductor disk laser influence of lateral lasing. *Applied Physics Letters*, 100(19), 2012.

[44] I. Vurgaftman, J. R. Meyer, and L. R. Ram-Mohan. Band parameters for iii–v compound semiconductors and their alloys. *Journal of Applied Physics*, 89(11):5815–5875, 2001.

[45] P. Yeh. *Optical waves in layered media*. Wiley series in pure and applied optics. Wiley, 2005.

[46] 2007. Yokogawa Electric Corporation. *User's Manual, AQ6375 Optical Spectrum Analyzer.*

A. APPENDIX

The semiconductor structure of the OP-SDL used in this thesis is shown in table A.1.

Table A.1: Structure of the OP-SDL used in this thesis. Marking "Times 4 ↑" means that the section above is repeated 4 times. (QW is quantum well)

Compound	In %	Al %	n(2450 nm)	OPL (nm)	thickness (nm)
GaSb cap	0.0	0.0	3.875	116.25	30
AlAsSb window	0.0	100.0	3.158	315.83	100.00
AlGaAsSb Spacer	0.0	49.8	3.421	1025.40	299.73
AlGaAsSb barrier	0.0	34.4	3.534	70.68	20
InGaAsSb QW	35.2	0.0	4.087	38.83	9.5
AlGaAsSb barrier	0.0	34.4	3.534	70.68	20
InGaAsSb QW	35.2	0.0	4.087	38.83	9.5
AlGaAsSb barrier	0.0	34.4	3.534	70.68	20
InGaAsSb QW	35.2	0.0	4.087	38.83	9.5
AlGaAsSb barrier	0.0	34.4	3.534	70.68	20
AlGaAsSb Spacer	0.0	49.8	3.421	825.79	241.39
AlGaAsSb barrier	0.0	34.4	3.534	70.68	20
InGaAsSb QW	35.2	0.0	4.087	38.83	9.5
AlGaAsSb barrier	0.0	34.4	3.534	70.68	20
InGaAsSb QW	35.2	0.0	4.087	38.83	9.5
AlGaAsSb barrier	0.0	34.4	3.534	70.68	20
InGaAsSb QW	35.2	0.0	4.087	38.83	9.5
AlGaAsSb barrier	0.0	34.4	3.534	70.68	20
					Times 4 ↑
AlGaAsSb Spacer	0.0	49.8	3.421	1025.40	299.73
AlAsSb DBR	0.0	100.0	3.158	612.50	193.93
GaSb DBR	0.0	0.0	3.875	612.50	158.06
AlAsSb DBR	0.0	100.0	3.158	612.50	193.93
					Times 21 ↑
GaAs buffer	0.0	0.0	3.875	387.51	100.00
n-GaAs subs.					